Chronic stress impairs autoinhibition in neurons of the locus coeruleus to increase asparagine endopeptidase activity

Hiroki Toyoda[1,2, †,*], Doyun Kim[3,†], Byeong Geon Koh[3], Tomomi Sano[4], Takashi Kanematsu[4], Seog Bae Oh[3,5,*], and Youngnam Kang[6,*]

[†]These authors contributed equally to this work.

[1]Department of Oral Physiology, Graduate School of Dentistry, Osaka University, Osaka 565-0871, Japan

[2]Department of Physiology, School of Dentistry, Aichi Gakuin University, Nagoya 464-8650, Japan

[3]Department of Neurobiology & Physiology, School of Dentistry and Dental Research Institute, Seoul National University, Seoul 03080, Republic of Korea

[4]Department of Cell Biology, Aging Science, and Pharmacology, Faculty of Dental Science, Kyushu University, Fukuoka 812-8582, Japan

[5]ADA Forsyth Institute, Cambridge MA, 02142, USA

[6]Department of Behavioral Sciences, Graduate School of Human Sciences, Osaka University, Osaka 565-0871, Japan

∗Correspondence:

Youngnam Kang: kang.yn.923@osaka-u.ac.jp

Department of Behavioral Sciences, Graduate School of Human Sciences, Osaka University, 1-2 Yamadaoka, Suita, Osaka 565-0871, Japan

Seog Bae OH: odolbae@snu.ac.kr

Department of Neurobiology & Physiology, School of Dentistry and Dental Research Institute, Seoul National University, Seoul 03080, Republic of Korea

Hiroki Toyoda: toyoda@dpc.agu.ac.jp

Department of Physiology, School of Dentistry, Aichi Gakuin University, Nagoya 464-8650, Japan

Abstract

Impairments of locus coeruleus (LC) are implicated in anxiety/depression and Alzheimer's disease (AD). Increases in cytosolic noradrenaline (NA) concentration and MAO-A activity initiate the LC impairment through production of NA metabolite, 3,4-dihydroxyphenyl-glycolaldehyde (DOPEGAL), by MAO-A. However, how NA accumulates in soma/dendritic cytosol of LC neurons has never been addressed despite the fact that NA is virtually absent in cytosol while NA is produced exclusively in cytoplasmic vesicles from dopamine by dopamine-β-hydroxylase. Since re-uptake of autocrine-released NA following spike activity is the major source of NA accumulation, we investigated whether and how chronic stress can increase the spike activity accompanied by NA-autocrine. Overexcitation of LC neurons is normally prevented by the autoinhibition mediated by activation of α2A-adrenergic receptor (AR)-coupled inwardly rectifying potassium-current (GIRK-I) with autocrine-released NA. Patch-clamp study revealed that NA-induced GIRK-I in LC neurons was decreased in chronic restraint stress (RS) mice while a similar decrease was gradually caused by repeated excitation. Chronic RS caused internalization of α2A-ARs expressed in cell membrane in LC neurons and decreased protein/mRNA levels of α2A-ARs/GIRKs in membrane fraction. Subsequently, chronic RS increased the protein levels of MAO-A, DOPEGAL-induced asparagine endopeptidase (AEP) and tau N368. These results suggest that chronic RS-induced overexcitation due to the internalization of α2A-ARs/GIRK is accompanied by $[Ca^{2+}]_i$ increases, subsequently increasing Ca^{2+}-dependent MAO-A activity and NA-autocrine. Thus, it is likely that internalization of α2A-AR increased cytosolic NA, as reflected in AEP increases, by facilitating re-uptake of autocrine-released NA. The suppression of α2A-AR internalization may have a translational potential for anxiety/AD treatment.

Keywords: locus coeruleus; α2A adrenergic receptor; GIRK; autoinhibition; MAO-A; AEP

Background

Locus coeruleus (LC) is implicated in anxiety and depression (*Itoi and Sugimoto, 2010*), and is often the first place where Alzheimer's disease (AD)-related pathology appears (*Mather and Harley, 2016*). Noradrenaline (NA) is known to inhibit amyloid-induced oxidative stress, and caspase activation in cortex/hippocampus (*Counts and Mufson, 2010*). Thus, the impairment of LC-noradrenergic system is potentially involved in the AD pathogenesis (*Ross et al., 2015; Chen et al., 2022*).

It was reported that cytosolic NA in the soma/dendrites of LC neurons is degraded by monoamine oxidase A (MAO-A) into 3,4-dihydroxyphenyl-glycolaldehyde (DOPEGAL) (*Burke et al., 1999*), which generates apoptotic free radicals (*Burke et al., 1998*) and activates asparagine endopeptidase (AEP) to produce Aβ and hypephosphorylated tau, consequently leading to AD (*Burke et al., 1999; Kang et al., 2020*). However, there appears normally no NA except dopamine in the cytosol of LC neurons because NA is produced exclusively in cytoplasmic vesicles by dopamine-β-hydroxylase (DBH) (*Potter and Axelrod, 1963*) from dopamine which is taken up into cytoplasmic vesicles by vesicular monoamine transporter type 2 (VMAT2).

LC neurons release NA following action potential not only from the axon terminals but also from their cell bodies as autocrine (*Huang et al., 2007*), and autocrine-released NA activates α2A adrenergic receptor (α2A-AR) expressed on the soma/dendrites (*Aoki et al., 1994*), resulting in activation of α2-AR-coupled inwardly rectifying K^+ (GIRK) channel (*Arima et al., 1998*) to cause autoinhibition (spike-afterhyperpolarization) (*Williams et al., 1985*). Thus, overexcitation of LC neurons is normally prevented by the autoinhibition.

As autocrine-released NA is taken up by NA-transporter (NAT) (*Torres et al., 2003*), uptaken-NA may be the only source of free NA to be metabolized by MAO-A in the cytosol of LC neurons. However, the amount of free NA to be metabolized by MAO-A in the cytosol is thought to be very small due to a much lower affinity of NA to MAO-A compared to VMAT2 (*Costa, 2012*). Therefore, it is not clear how free NA to be metabolized by MAO-A is increased in the soma/dendites of LC neurons in AD pathogenesis. Because the passive NA-leakage occurs from cytoplasmic vesicles in a manner that achieves a dynamic equilibrium with active NA-storage into cytoplasmic vesicles by VMAT2 (*Eisenhofer et al., 2004*), increased NA-uptake by NAT in response to increased NA-autocrine following $[Ca^{2+}]_i$ increases or overexcitation may increase free NA by facilitating the passive NA-leakage from cytoplasmic vesicles. Furthermore, the affinity of MAO-A for NA may be modifiable as MAO-A activity

96 is Ca^{2+}-dependent (*Cao et al., 2007*). Then, a question arises whether or not impairment of
97 autoinhibition that causes overexcitation and $[Ca^{2+}]_i$ increases can consequently increase AEP
98 activity through the production of DOPEGAL.

99 Neuronal activity in LC neurons is transiently increased by stress (*Valentino and Foote,*
100 *1988*) through activation of corticotropin releasing factor (CRF) receptor (*Valentino et al.,*
101 *1983; McCall et al., 2015*) together with glutamate receptors (*Valentino et al., 2001*). However,
102 even if firing activity is increased by synaptic activation (*Barcomb et al., 2022*), autoinhibition
103 would occur to suppress overexcitation in LC neurons. Nevertheless, it is known that long-
104 term overexcitation due to chronic stress ultimately causes degeneration of LC neurons
105 (*Kitayama et al., 2004*). Then, this raises an important question whether and how stress impairs
106 autoinhibition to cause sustained overexcitation. The whole mechanisms for the impairment
107 of LC would be revealed by solving these questions. Here we examined whether the
108 autoinhibition mediated by α2A-AR-coupled GIRK-I is impaired by overexcitation in LC
109 neurons or chronic stress, to clarify the mechanisms for NA accumulation and/or MAO-A
110 activity increase.

111

112 Results

113 Spike frequency adaptation in LC neurons is mediated by α2-AR-coupled GIRK channel

114 LC neurons invariably display spike-frequency adaptation (**Figure 1A, B**). We have
115 hypothesized that the autoinhibition would occur following respective spike firing and
116 contribute to the generation of the spike-frequency adaptation and the afterhyperpolarization
117 seen at the offset of current pulses.

118 When the cumulative number of spikes was plotted against the elapsed time from the
119 onset of the current pulse every 50 ms, the cumulative spike number increased non-linearly in
120 a saturation manner (**Figure 1C**). This non-linear relationship was fitted with a saturation
121 curve defined by Monod equation (see Extended Methods and Materials) in order to quantify
122 the spike-frequency adaptation. Because there was no significant difference in ***b*** between the
123 two groups of spike trains, the profile of the normalized cumulative spike number vs the elapsed
124 time remains the same regardless of firing frequency, suggesting that spike-frequency
125 adaptation occurs in the same way.

126 The spike-frequency adaptation observed was almost completely abolished by a blocker
127 of α2-AR, atipamezole (**Figure 1D, E**), which subsequently largely decreased pulse-
128 afterhyperpolarization (pulse-AHP) (**Figure 1D, E**, blue and red stars). The cumulative spike

129 number increased non-linearly in a saturation manner in the control condition while it increased
130 almost in a linear manner after atipamezole application (**Figure 1F**). In the relationship
131 between ***a*** and ***b*** examined in LC neurons, atipamezole invariably and significantly shifted both
132 ***a*** and ***b*** in a larger direction, and there was a significant difference in the relationship between
133 ***a*** and ***b*** (**Figure 1G**).
134 Bath application of NA induced a GIRK-I in response to the ramp pulse (**Figure 1H**, red
135 trace) whereas addition of atipamezole to NA almost completely abolished the NA-induced
136 GIRK-I (**Figure 1H**, blue trace), showing that GIRK-I reversed at –97 mV. The amplitudes of
137 the inward component of NA-induced GIRK-I were invariably larger than those of the outward
138 component, consistent with the inwardly rectifying property of GIRK-I. Atipamezole
139 significantly decreased the amplitudes of the inward and outward components (**Figure 1I**).
140 Taken together, NA-autocrine is likely to be caused following respective spikes in the LC
141 neuron and NA is accumulated around the LC neuron to activate α2-AR-coupled GIRK
142 channels, to cause spike-frequency adaptation by enhancing AHP.
143
144 **Ca^{2+}-dependent rundown of NA-induced GIRK-I in LC neurons**
145 In PC12 cells, heterologously expressed α2A-ARs undergo internalization following agonist
146 application (*Taraviras et al., 2002*). Such internalization of α2A-ARs would result in an
147 abolishment of GIRK-I or desensitization given the functional coupling between α2A-AR and
148 GIRK as in LC noradrenergic neurons. However, in LC neurons, NA-induced GIRK-I showed
149 almost no rundown/desensitization after repeating the ramp pulse 20 times in the persistent
150 presence of NA (**Figure supplement 1A-D**). Then, we next examined whether GIRK-I shows
151 rundown under the condition of "increased excitability" or increased $[Ca^{2+}]_i$, because
152 acute/chronic stress increases the excitability of LC neurons (*Borodovitsyna et al., 2018;*
153 *Campos-Lira et al., 2018*) and various channels/receptors are known to be internalized in a
154 Ca^{2+}-dependent manner (*Beattie et al., 2000; Aziz et al., 2012; Zaccor et al., 2020*).
155 To examine the Ca^{2+}-dependency of the rundown of GIRK-I, the respective ramp
156 pulses to evoke GIRK-I were preceded by various pulse trains which can induce Ca^{2+} currents
157 differentially (compare **Figure supplement 1F** and **Figure 2B**). After examining various pulse
158 protocols (**Figures supplement 1 and 2**), the best protocol to induce a prominent rundown of
159 GIRK-I was as follows (shown in **Figure 2B)**. First, bath application of NA induced GIRK-I
160 (**Figure 2A,** red trace; 2) that showed the inwardly rectifying profile as revealed by subtraction
161 of the control response from that obtained after NA application (**Figure 2D**, red trace; 2−1).

162 Subsequently, the combined command pulse (a set of 5 trains of 20 pulses followed by a ramp
163 pulse; **Figure 2B**, upper trace) was applied every minute. The positive pulse trains evoked
164 large inward Ca^{2+} currents in the presence of extracellular 30 mM TEA (**Figure 2B**, lower
165 traces) whereas similar trains of the same positive pulse hardly induced Ca^{2+} currents when
166 applied in the absence of TEA (**Figure supplement 1F**, lower trace). With repetition of the
167 combined command pulse 20 times, the NA-induced GIRK-I (**Figure 2C**, red trace; 2) was
168 decreased to almost the same current as the control response (**Figure 2C**, blue trace; 3). Indeed,
169 no GIRK-I remained after 20 times repetition of the combined command pulse as revealed by
170 the subtraction between trace 1 and trace 3 (**Figure 2D**, blue trace; 3−1). Both the amplitudes
171 of the inward and outward components of the NA-induced GIRK-I promptly decreased to zero
172 along with repetition of the combined command pulse (**Figure 2E**, blue and red circles; **Figure**
173 **2F**). Thus, it is likely that NA-induced GIRK-I displays a marked rundown in a Ca^{2+}-dependent
174 manner. Furthermore, we confirmed that these rundowns were completely dependent on the
175 number and application timing of the command pulse in the presence or absence of TEA
176 (compare **Figure 2** with **Figures supplement 1 and 2**). Depending on the absence or presence
177 TEA, the single application of a set of 10 trains of 20 pulses differentially (slightly or
178 moderately, respectively) induced the rundown of NA-induced GIRK-I (compare **Figure**
179 **supplement 1E-J** and **Figure supplement 2A-E**). By contrast, the repetitive application of a
180 single train of 20 positive pulses in the presence of TEA markedly facilitated the rundown of
181 NA-induced GIRK-I (**Figure supplement 2F-K**). The relationship between the number of
182 spikes (i.e., positive pulse) and $[Ca^{2+}]_i$ was obtained by measuring Ca^{2+} transients using fura-2
183 (**Figure supplement 3**).
184 To investigate the effects of the rundown of GIRK-I on the spike-frequency adaptation,
185 spike trains were examined before and after the voltage-clamp experiment (**Figure 2A-F**).
186 After the rundown of GIRK-I was observed in the voltage-clamp experiment, the spike-
187 frequency adaptation was absent in the current clamp experiment, and the pulse-ADP was
188 largely reduced (**Figure supplement 4A-D**). The cumulative spike number that increased non-
189 linearly in a saturation manner before rundown of GIRK-I increased almost in a linear manner
190 after rundown of GIRK-I (**Figure supplement 4E, F**). Thus, the rundown of GIRK-I
191 invariably resulted in an abolishment of spike-frequency adaptation, similar to the effects of
192 atipamezole on spike-frequency adaptation (**Figure 1**). Therefore, it is likely that Ca^{2+}
193 increases can cause the rundown of NA-induced GIRK-I and almost abolished the spike-
194 frequency adaptation, leading to an increase in the excitability of LC neurons. These

195 observations suggest that $[Ca^{2+}]_i$ increases cause rundown of NA-induced GIRK-I to suppress
196 autoinhibition, leading to excitability increases that cause further increases in $[Ca^{2+}]_i$ to further
197 cause a rundown of the GIRK-I.
198 It was also examined whether the rundown of NA-induced GIRK-I can be caused solely
199 by $[Ca^{2+}]_i$ increases without activation of α2-AR. We found that NA-induced GIRK-I
200 subjected to the combined command pulse 20 times in the presence of atipamezole was
201 significantly restored after washout of atipamezole in the presence of NA (**Figure supplement**
202 **5A-D**). This observation indicates that GIRK-I were not downregulated solely by $[Ca^{2+}]_i$
203 increases without activation of α2-AR, clearly revealing that both the activation of α2-AR and
204 $[Ca^{2+}]_i$ increases are necessary to cause the downregulation of GIRK-I. In agreement with this
205 result, the spike-frequency adaptation reflecting the autoinhibition was also preserved in spite
206 of $[Ca^{2+}]_i$ increases as long as activation of α2-AR is prevented (**Figures supplement 5E-J**).
207 We further examined whether the rundown of NA-induced GIRK-I can be prevented by the
208 presence of a GIRK channel blocker, tertiapin-Q. GIRK channel blockade did not prevent the
209 rundown of NA-induced GIRK currents following $[Ca^{2+}]_i$ increases (**Figure supplement 6A-**
210 **H**). In agreement with this result, the spike-frequency adaptation was not preserved by with
211 the blockade of GIRK channels during $[Ca^{2+}]_i$ increases (**Figure supplement 6I-N**). These
212 findings showed that α2-AR blockade but not GIRK blockade prevented the rundown of NA-
213 induced GIRK-I following $[Ca^{2+}]_i$ increases. Taken together, it is suggested that the rundown
214 of NA-induced GIRK-I may be brought about by the internalization of α2-AR in a Ca^{2+}-
215 dependent manner, regardless of opening or closing of GIRK channels.
216
217 **β-Arrestin is involved in the rundown of NA-induced GIRK-I**
218 We further examined whether the internalization of α2-AR is involved in the rundown of NA-
219 induced GIRK-I or not. As β-arrestin/AP2 complex is known to be involved in the agonist-
220 dependent internalization of GPCR (*DeGraff et al., 1999; Cottingham et al., 2011*), we
221 examined the effects of barbadin, which prevents AP2 from binding with β-arrestin by forming
222 barbadin/AP2 complex, on the rundown of NA-induced GIRK-I. With the patch pipettes filled
223 with barbadin-including internal solution, it was examined whether NA-induced GIRK-I
224 displays rundown in response to the same combined command pulse (**Figure 2H**, upper trace)
225 as that in the control experiment (**Figure 2B**, upper trace). The NA-induced GIRK-I (**Figure**
226 **2G-I**, red traces) was hardly decreased (**Figure 2H, I**, blue traces) after repeating the combined
227 pulse 20 times, in contrast to the control rundown (**Figure 2C, D**). Barbadin largely suppressed

228 the rundown of the both components of GIRK-I (**Figure 2J, K**). These results suggest that the
229 rundown of NA-induced GIRK-I is caused by the internalization of α2-AR-coupled GIRK
230 channels.
231
232 **Restraint stress alters α2A-AR expression in LC neurons**
233 We next investigated whether the expression of α2A-AR is altered in LC neurons by applying
234 restraint stress (RS) to mice. After mice were subjected to daily 12-h RS for 3 days followed
235 by non-stress condition for 2 days, the immunoreactivity for α2A-ARs (see **Figure supplement**
236 **7**) seen along the membrane of TH-positive LC neurons was apparently lower compared to the
237 control (**Figure 3A, B**). Consistent with this observation, Western blot analysis revealed
238 significantly lower protein levels of α2A-ARs in LC neurons obtained after 3-day RS compared
239 to the control (**Figure 3C**). Especially when α2A-ARs expression was examined in the
240 membrane fraction identified using Na^+/K^+-ATPase, the immunoreactivity for α2A-ARs
241 expression was apparently lower in LC neurons of RS mice than in those of the control mice
242 (**Figure 3D, E**; *, compare the rightmost lower panels). Consistent with this observation,
243 Western blot analysis revealed a significantly lower protein level of α2A-ARs in the membrane
244 fraction of LC neurons of RS mice compared to the control whereas there was no significant
245 difference in the cytosol between the control and RS mice (**Figure 3F, G**). Thus, the
246 internalization of α2A-ARs is not necessarily accompanied by increases in cytosolic levels of
247 α2A-ARs because the internalized receptors are either recycled or degraded (*Koenig and Ikeda,*
248 *1996; Takei et al., 1996*).
249
250 **RS reduces NA-induced GIRK-I**
251 As 3-day RS caused the internalization or downregulation of α2A-ARs, we next examined if
252 the daily 12-h RS for up to 5 days can differentially cause reductions of NA-induced GIRK-I
253 in LC neurons. NA-induced GIRK-I decreased with an increase in the RS period (**Figure 4A-**
254 **E**). The amplitudes of inward and outward components of GIRK-I decreased with the increase
255 in the period of RS (**Figure 4F, G**), in a way that is described by a saturation function (red
256 interrupted lines). The amplitudes of inward and outward components of GIRK-I in 1-day
257 mice were significantly smaller than those of the control mice, and those in 3-day RS mice
258 were significantly smaller than those in 1-day RS mice while no significant difference in those
259 between 3-day and 5-day RS mice (**Figure 4F, G**). Thus, the downregulation of GIRK-I was
260 increased as RS period is increased, but in a saturation manner.

261 Quantitative PCR analysis revealed that LC neurons expressed much higher mRNA
262 level of α2A-AR than that of α2C-AR (**Figure 4H**) and also expressed higher mRNA level of
263 GIRK1 compared to GIRK2 while GIRK3 was hardly expressed (**Figure 4I**). Consistent with
264 the significant decreases in NA-induced GIRK-I in the mice subjected to 3-day RS, mRNA
265 levels of α2A-AR, GIRK1 and GIRK2 in mice subjected to 3-day RS were significantly smaller
266 than those of the control mice (**Figure 4J-L**). Thus, RS downregulated the
267 expression/production of α2A-AR-coupled GIRK1 prominently in LC neurons.
268

269 **Histological and biochemical changes in LC neurons after 5-day RS**

270 Next, immunohistochemical experiments demonstrated that 5-day RS appeared to slightly
271 increase the expressions of TH and MAO-A in LC neurons (**Figure supplement 8A**).
272 Furthermore, AEP expression also appeared to increase in cytosol after 5-day RS compared to
273 the control (**Figure supplement 8B**). Because TH catalyzes the rate limiting step in the
274 synthesis of catecholamines, if the RS enhances TH activity, free NA concentration in LC
275 neurons would be directly and greatly increased. Therefore, we first carefully examined
276 whether TH is really upregulated in RS mice or not by performing Western blot analysis. No
277 significant increase in the protein level of TH was observed in 5-day RS mice compared to the
278 control (**Figure 5A**, upper panel; **Figure 5B**). This result clearly indicates that TH activity was
279 not significantly upregulated in 5-day RS mice, in spite of the TH immunohistochemical
280 experiment. We further examined whether protein levels of MAO-A and AEP are increased
281 or not by 5-day RS. Western blot analysis revealed significant increases in the protein levels
282 of MAO-A (**Figure 5A**, lower panel; **Figure 5C**) and of pro-AEP and active AEP (**Figure 5D-**
283 **F**) in LC neurons after 5-day RS compared to the control. Western blot analysis also revealed
284 a significant increase in the expression of tau and tau N368 fragment after 5-day RS (**Figure**
285 **5G-I**). Thus, an increased activity of active AEP caused a production of tau N368 fragments
286 as observed at 37 and 35 kDa (**Figure 5G**), which is consistent with a previous report (*Zhang*
287 *et al., 2014*). Relative protein levels of the tau N368 fragments (**Figure 5I**) were the mean
288 values obtained from the two band intensities, which may reflect the two N-terminal fragments
289 (upper and lower bands) generated by AEP cleavage at Asn-368 of the 4 and 3 repeat-tau
290 isoforms, respectively (*Goedert et al., 1989*). Finally, Y-maze test revealed that 5-day RS
291 decreased spatial memory (**Figure supplement 9**).
292

293 ## Discussion

294 We have found that LC neurons display spike-frequency adaptation which is caused by the
295 autoinhibition mediated by α2A-AR-coupled GIRK-I following respective spikes (**Figure 1**)
296 and that α2A-AR-coupled GIRK-I showed Ca^{2+}-dependent rundown due to the internalization
297 of α2A-AR (**Figure 2**, **Figure supplement 5A-D** and **Figure supplement 6E-H**), leading to
298 the abolishment of spike-frequency adaptation and the excitability increase (**Figure**
299 **supplement 4**). Immunohistochemical examination and Western blot analysis revealed that
300 α2A-AR expression in cell membrane was decreased following RS (**Figures 3 and 4J**).
301 Consistently, NA-induced GIRK-I was decreased in LC neurons with an increase in the period
302 of RS (**Figure 4A-G**). Following chronic RS, protein levels of MAO-A, pro-/active-AEP, and
303 tau and tau N368 fragment were significantly increased (**Figure 5A, C-I**).

304 Based on these results, we propose a novel mechanism for how chronic RS impairs
305 autoinhibition and increases cytosolic free NA to be metabolized by enhanced Ca^{2+}-dependent
306 MAO-A activity, to consequently increase AEP activity and produce tau N368 protein (**Figure**
307 **6**). In non-stress mice, autocrine released NA is slowly taken up by NAT after binding to α2A-
308 ARs to cause autoinhibition (**Figure 6A**), while in chronic RS mice, autocrine-released NA
309 may be directly and rapidly taken up by NAT due to the absence (internalization) of α2A-ARs
310 (**Figure 6B**). Such increased rate of re-uptake of NA by NAT would increase free NA
311 concentration by facilitating the leakage of NA from cytoplasmic vesicles in the cell body,
312 which would be metabolized by upregulated MAO-A activity to DOPEGAL, as revealed by
313 the increased activity of AEP in chronic RS mice (**Figure 6B**). It may be further necessary to
314 perform enzymatic assay to better demonstrate the AEP and MAO-A activities.

315

316 **Spike frequency adaptation**

317 LC neurons display spike-frequency adaptation. The mechanism for the spike-frequency
318 adaptation may be different among neurons while M currents are usually responsible for the
319 adaptation in hippocampal pyramidal neurons (*Aiken et al., 1995*). In LC neurons, the spike-
320 frequency adaptation was mediated by α2A-AR-coupled GIRK-I as the spike-frequency
321 adaptation was abolished by atipamezole (**Figure 1D-G**) and by causing the rundown of GIRK-
322 I (**Figure supplement 4**). These results suggest that autocrine NA release following respective
323 spikes activated α2A-ARs expressed in the soma/dendrites of LC neurons, and subsequently
324 activated α2A-AR-coupled GIRK-I to cause autoinhibition as spike-frequency adaptation.
325 Thus, spike-frequency adaptation clearly reflects NA-autocrine.

326

327 **Rundown of α2A-AR-coupled GIRK-I**

328 α2A-AR-coupled GIRK-I displayed Ca^{2+}-dependent rundown in the presence of agonist. The
329 degree and time course of rundown of α2A-AR-coupled GIRK-I were dependent on the number
330 and timing of positive pulses applied under voltage-clamp condition to cause Ca^{2+} currents
331 (**Figure 2A-F** and **Figures supplement 1E-J, 2, 3**). Given the Ca^{2+}-dependency of the
332 rundown of autoinhibition, the excitability of LC neurons would increase as LC neurons were
333 excited more such as under RS condition, resulting in a vicious cycle between excitability
334 increase accompanied by $[Ca^{2+}]_i$ increase and rundown of autoinhibition/Ca^{2+}-dependent
335 internalization of α2A-ARs.

336

337 **Internalization of α2A-ARs**

338 Activation of GPCR by agonist binding usually causes the formation of GPCR/β-arrestin
339 complexes. Subsequently, the GPCR/β-arrestin complex is assembled through the interaction
340 between β-arrestin and AP2 in clathrin-coated pits (CCPs), which is formed by the association
341 of AP2 with phosphatidylinositol 4,5-bisphosphate (PIP2) at the plasma membrane, leading to
342 endocytosis of GPCRs (*Pierce and Lefkowitz, 2001*). PIP2 is locally produced from the
343 membrane phosphatidylinositol (PI) by PI4/PIP5 kinases in a Ca^{2+}-dependent manner
344 (*Sarmento et al., 2014*). Barbadin prevented the stable formation of sufficient GPCR/β-
345 arrestin/AP2 complexes in CCPs as barbadin prevents AP2 from binding with β-arrestin by
346 forming barbadin/AP2 complex, thereby hampering GPCR internalization (*Beautrait et al.,*
347 *2017*). In the present study, intracellular barbadin effectively suppressed the rundown of
348 GIRK-I (**Figure 2G-K**), indicating that the rundown of GIRK-I was caused by the
349 internalization of α2A-ARs in LC neurons.

350

351 **Chronic RS increases the activities of MAO-A and pro-/active-AEP in the cell body**

352 Chronic cold stress reduced α2-AR mediated inhibition of LC neurons (*Jedema et al., 2008*),
353 and chronic social stress downregulated α2-ARs in the LC (*Flugge, 1996*). Our present results
354 were consistent with those previous findings: Following RS, α2A-ARs expression was
355 decreased due to the internalization of α2A-ARs (**Figure 3**), together with the decreases in NA-
356 induced GIRK-I (**Figure 4A-G**) which mediates the autoinhibition. As long as RS persists, the
357 impairment of autoinhibition leads to the persistent overexcitation in LC neurons. This would
358 further increase NA-autocrine, because respective spikes were accompanied by NA-autocrine

359 as reflected in spike-frequency adaptation or autoinhibition.

360 As extracellular NA is mostly taken up into cytosol by NAT (*Torres et al., 2003*), it is
361 likely that under chronic RS the increased autocrine-released NA is directly and more rapidly
362 taken up by NAT due to the absence of α2A-ARs (**Figure 6B**). Such an increase in the rate of
363 NA uptake by NAT is similar to the effects of uptake inhibitor of transmitter ligand on the
364 activity of receptors. After re-uptake of NA by NAT, a large portion of NA in the cytosol is
365 restored in cytoplasmic vesicles by VMAT2 while only a small portion of NA can escape from
366 VMAT2 to be metabolized by MAO-A (*Eisenhofer et al., 1992*), because VMAT2 has a much
367 higher affinity for NA than MAO-A (*Bloom, 2006; Costa, 2012*). However, there is an
368 additional component of NA to be metabolized by MAO-A, as NA can leak from cytoplasmic
369 vesicles into cytosol (*Eisenhofer et al., 2004*). When re-uptake of NA by NAT is facilitated
370 due to the internalization of α2A-ARs in response to NA-autocrine, active NA storage into
371 cytoplasmic vesicles by VMAT2 would increase. Then, the rate of NA leakage from
372 cytoplasmic vesicles would also increase because passive NA leakage from cytoplasmic
373 vesicles and active NA storage into cytoplasmic vesicles by VMAT2 are in a dynamic
374 equilibrium in cytoplasmic vesicles (*Eisenhofer et al., 2004*). Subsequently, such increases in
375 the rate of NA leakage would result in increases in a MAO-A metabolite, DOPEGAL
376 (*Goldstein, 2021*) (**Figure 6B**). Indeed, it has previously been demonstrated that a partial
377 inhibition of NAT in human subjects reduced the original level of a derivative of DOPEGAL
378 (3,4-dihydroxyphenylglycol; DHPG) in CSF by more than 50% (*Kielbasa et al., 2015*). Thus,
379 free NA to be metabolized by MAO-A would be increased when autocrine-released NA is
380 taken up by NAT. On the other hand, it is also known that the decreased VMAT2 levels,
381 generated in VMAT2 heterozygote mice, increased the vulnerability of nigral dopamine
382 neurons to MPTP (*Takahashi et al., 1997*). Thus, it is conceivable that NA leakage for free
383 NA accumulation is influenced by both NAT or VMAT2.

384 Therefore, under the chronic RS condition, more NA leaked from cytoplasmic vesicles is
385 likely to be metabolized by MAO-A, which activity is enhanced Ca^{2+}-dependently and by
386 chronic RS (*Cao et al., 2007*) (**Figures 5A, C and 6B**), to DOPEGAL compared to the control
387 condition, as revealed by the increased protein levels of pro-AEP and active-AEP (**Figure**
388 **supplement 8B and Figure 5D-F**). Thus, re-uptaken NA by NAT may largely be degraded to
389 DOPEGAL by the increased activity of MAO-A. Subsequently, DOPEGAL converts pro-AEP
390 into active-AEP to produce tau N368 protein (**Figure 5G-I**).

391 It has never been addressed how DOPEGAL production was caused in the cell body
392 of LC neurons while the DOPEGAL production in the cell bodies of LC neurons is well
393 established in AD patients (*Burke et al., 1999; Kang et al., 2020*) and in transgenic AD model
394 mice (*Kang et al., 2020*). We demonstrated for the first time that 5-day RS can impair the
395 autoinhibition by causing the internalization of α2A-AR and consequently induces active-AEP
396 to produce tau N368 fragment. Indeed, 5-day RS induced spatial memory impairment-like
397 responses in mice when assessed using Y-maze test (**Figure supplement 9**) while anxiety-like
398 behavior was also induced in mice after 3-day RS when assessed using an elevated plus maze
399 test (figure not shown), both suggesting an impairment of LC neurons. It is likely that, in
400 addition to NAT inhibitor, the suppression of the internalization of α2A-AR has a strong
401 translational potential for developing drugs that prevent the degeneration of LC.
402
403 **Limitations of this study**
404 One may argue against the usage of 3-week-old juvenile mice to study the neurodegenerative
405 disorder which is normally found in aged ones. However, a stringent autoinhibition together
406 with potent NAT activity were previously demonstrated in adult rats using intracellular
407 recordings (*Williams et al., 1985*). Thus, regardless of the age of mice, LC neurons showed
408 the autoinhibition that is mediated by the activity of α2A-AR-coupled GIRK channels. We
409 also confirmed that spike-frequency adaptation reflecting autoinhibition can be induced in adult
410 mice as prominently as in juvenile mice regardless of sexes (**Figure supplement 10**), although
411 we did not investigate the sex differences in RS effects (*Leistner and Menke, 2020*). The
412 downregulation of autoinhibition by the internalization of α2A-AR is agonist- and Ca^{2+}-
413 dependent regardless of the age of mice. However, it is not known if there is any difference in
414 the susceptibility of α2A-AR internalization to RS between juvenile and aged mice. Thus, a
415 further study may be necessary to examine if autoinhibition in LC neurons is more easily
416 downregulated in aged mice compared to juvenile ones.
417 It has also been reported that re-uptake of NA by NAT in LC neurons may decrease
418 with age (*Sanders et al., 2005; Mitchell et al., 2017*). However, NAT expression in LC in 3-
419 week-old juvenile mice was only slightly larger (by 4%) than in adult mice although the
420 difference was significant (*Mitchell et al., 2017*). Potent NAT activity stringently affecting
421 autoinhibition was reported in adult rats (*Williams et al., 1985*). Furthermore, partial inhibition
422 of NAT in human subjects largely reduced the original level of a derivative of DOPEGAL in
423 CSF as described above. Thus, based on the present study, it is likely that increased re-uptake

424 of NA by NAT following excessive NA-autocrine in the absence of α2A-AR, induced in
425 response to chronic RS, resulted in the increase in active-AEP and subsequent production of
426 tau N368. However, a further experiment to directly assess NAT activity would be necessary
427 to firmly justify our hypothesis.

428 To further validate the mechanisms which we have proposed in the present study
429 (Figure 6), direct quantification of the relationship between α2A-AR internalization and
430 increased cytosolic NA levels may be desirable. However, at present, the quantification of
431 such connection may not be possible because there appears to be no fluorescence probe to label
432 cytosolic NA. None of NA fluorescence probes, such as NS521, BPS3 or GRAB-NE, is
433 applicable to detect cytosolic free NA because NS521 and BPS3 anchor on plasma membrane
434 and GRAB-NE is dependent on GPCR activation (*Hettie and Glass, 2014; Feng et al., 2019;*
435 *Mao et al., 2023*).
436

437 **Conclusion**

438 Our study unveiled the cellular mechanism for the degeneration of LC neurons under chronic
439 RS as follows: Chronic RS impaired the autoinhibition in LC neurons by inducing Ca^{2+}- and
440 agonist-dependent internalization of soma/dendritic α2A-AR coupled with GIRK channels.
441 This subsequently caused overexcitation/$[Ca^{2+}]_i$ increases and increased Ca^{2+}-dependent
442 MAO-A activity and active AEP activity, leading to a production of tau N368 fragment
443 together with an impairment of spatial memory. These results clearly indicate that chronic RS
444 increases cytosolic free NA to be metabolized by MAO-A, presumably by facilitating the re-
445 uptake of autocrine-released NA due to the absence/internalization of α2A-AR. Thus, in
446 addition to NAT inhibitor, the suppression of α2A-AR internalization may have a strong
447 translational potential for developing drugs that prevent the degeneration of LC. However, the
448 present mechanism must be proven to be valid in adult or old mice, to validate its involvement
449 in the pathogenesis of anxiety/AD.
450

451 **Methods**

452 **Restraint stress**

453 Three-weeks-old male C57BL/6 mice (JAPAN HAMAMATSU SLC, Hamamatsu, Japan)
454 were used and housed at 24 ± 2°C. Food and water were available ad libitum. The mice in the
455 stressed groups were restrained in a modified 50 ml clear polystyrene conical centrifuge with

456 multiple air holes for ventilation. The mice were subjected to 12-h restraint stress (RS; 20:00
457 p.m. to 8:00 a.m. of the next day) for 1, 2, 3 and 5 days. In the previous study, the duration of
458 RS widely ranged from 0.5-h (*Gray et al., 2010*) to 24-h (*Chu et al., 2016*) while the RS with
459 the duration less than 12-h has been applied daily for a period (6-h for 2 weeks (*Sakaguchi and*
460 *Nakamura, 1990*); 8-h for up to 16 weeks (*Sugama et al., 2016*); 12-h for 2 days (*Zhang et al.,*
461 *2008*)). As the prolonged stress is known to be a potential risk factor for AD (*Bisht et al.,*
462 *2018*), the protocol of daily 12-h RS is relevant for the study of functional and cytological
463 disorders of LC neurons. Once the restraint ended, the mice were returned to their home cages
464 with access to food and water ad libitum. The control group remained in their home cages
465 without the restraint procedure.

466

467 **Slice preparation and electrophysiological recordings**

468 Slices were prepared from 3-weeks-old male C57BL/6 mice to investigate the effects of RS for
469 varying periods on GIRK-I, and from C57BL/6 mice of either sex at 16–23 postnatal days (PD)
470 to investigate the effects of $[Ca^{2+}]_i$ increases on GIRK-I, similar to our previous study (*Toyoda*
471 *et al., 2022*). Using an Axopatch 200B (MDS Analytical Technologies, Sunnyvale, CA),
472 whole-cell recordings were made from LC neurons that were viewed under Nomarski optics
473 (BX51WI; Olympus, Tokyo, Japan). LC neurons were identified immunohistochemically and
474 electrophysiologically as we previously reported (*Toyoda et al., 2022*). The internal solution
475 of the patch pipettes had the following ionic composition (in mM): 123 K-gluconate, 18 KCl,
476 10 NaCl, 2 $MgCl_2$, 2 ATP-Na_2, 0.3 GTP-Na_3, 10 HEPES, and 0.2 EGTA; pH 7.3. The
477 membrane potential values given in the text were corrected for the junction potential (10 mV)
478 between the internal solution for the whole-cell recording (negative) and the standard
479 extracellular solution. The pipette resistances were 4–6 MΩ. The series resistance was < 10
480 MΩ. All recordings were made at room temperature (RT). Records of currents and voltages
481 were low-pass filtered at 5 kHz (3-pole Bessel filter), digitized at a sampling rate of 10 kHz
482 (Digidata 1322A, MDS Analytical Technologies) and stored on a computer hard disk. Spike-
483 frequency adaptation was quantitatively estimated by fitting with a saturation curve defined by
484 Monod equation ($y = (\boldsymbol{a} * x) / (\boldsymbol{b} + x)$) with a saturation level (***a***) and a half saturation constant
485 (***b***). The amplitudes of inward and outward components of NA-induced GIRK-I were
486 measured at –130 mV and –60 mV.

487

488 **Procedure for immunohistochemical examination**

489 C57BL6/J male mice (4-5 weeks) were perfused transcardially with 5 ml of PBS, followed by
490 10 ml of a freshly prepared 4% paraformaldehyde in PBS. The whole brain including LC (–9
491 to –10 mm from bregma) was dissected out and immersed in 4% paraformaldehyde solution
492 for 4 h at 4°C fallowed by cryoprotection with 30% (w/w) sucrose in PBS.

493 Brainstem including LC regions was cut into 8-20 μm-thickness coronal sections on a
494 freezing microtome (Leica Microsystems, Wetzlar, Germany). To examine the distribution of
495 α2A-AR in LC neurons, mouse anti-TH (1:500; sc-25269, Santa Cruz Biotechnology, Santa
496 Cruz, CA, USA), rabbit anti-sodium potassium ATPase (1:1000; ab76020, Abcam, Cambridge,
497 MA, USA) and goat anti-α2A-AR (1:200; ab45871, Abcam) or rabbit anti-α2A-AR (1:500;
498 RA14110, Neuromics, Northfield, MN, USA) were used as primary antibodies, while cy5
499 donkey anti-mouse IgG (1:500; cy-2500, Vector Laboratories, Burlingame, CA, USA), FITC
500 donkey anti-rabbit IgG (1:500; 711-095-152, Jackson ImmunoResearch, West Grove, PA,
501 USA) and Cy3 donkey anti-goat IgG (1:500; 706-165-147, Jackson ImmunoResearch) were
502 used as secondary antibodies. We used the affinity purified IgG antibody for α2A-AR
503 immunohistochemistry, in which antibody specificity was ensured as examined previously
504 (*Stone et al., 1998; Tan et al., 2009*). To examine the expression in LC neurons, mouse anti-
505 TH (1:500) and rabbit anti-MAO-A (1:2000; ab126751, Abcam) were used as primary
506 antibodies, while FITC donkey anti-mouse IgG (1:500; 715-545-150; Jackson
507 ImmunoResearch) for TH and Cy3 donkey anti-rabbit IgG (1:2000; 711-165-152; Jackson
508 ImmunoResearch) were used as secondary antibodies. To examine the distribution of legumain
509 in LC neurons, mouse anti-legumain (1:200; sc-133234, Santa Cruz) and rabbit anti-DBH
510 (1:500; 22806, ImmunoStar, Hudson, WI, USA) were used as primary antibodies, while FITC
511 donkey anti-mouse IgG (1:500; 715-545-150, Jackson ImmunoResearch) and Cy3 donkey anti-
512 rabbit IgG (1:500; 711-165-152, Jackson ImmunoResearch) were used as secondary antibodies.
513 The slices were coverslipped with mounting media (H1000, Vector Laboratories), and sections
514 were visualized with a confocal microscope (LSM980, Carl Zeiss, Oberkochen, Germany) at
515 10x and 63x magnification.

516

517 **Western blot study**

518 Brain slices from the control and 5-day RS-treated mice were sectioned with vibratome
519 (VT1000P, (Leica Microsystems) to obtain 500 μm-thickness coronal sections containing LC

520 region (bregma –5.34 mm to –5.80 mm). We performed Western blot study only in 5-day RS
521 mice without examining in 3-day RS mice, under the assumption that for the degeneration-
522 related biochemical changes to reach sufficiently detectable levels, a high $[Ca^{2+}]_i$ condition due
523 to the rundown of GIRK-I have to be sustained for some period of time after the rundown of
524 GIRK-I reached a plateau level in 3-day RS mice (see Figure 4F, G). LC dissection was done
525 via micro punch using 1.5 mm biopsy punch (BP-15F, Kai medical, Gifu, Japan) bilaterally
526 under light microscope. Dissected LC were quickly frozen in liquid nitrogen and stored at
527 −80°C until processed. Because LC region was too small to collect sufficient tissue from one
528 mouse for the analysis, the punched LC tissues were collected from two to three mice to obtain
529 a protein lysate sample for each Western blotting analysis. LC tissues were homogenized by
530 bead homogenizer in T-PER™ Tissue Protein Extraction Reagent (78510, Thermo Fisher)
531 containing protease and phosphatase inhibitor cocktails (MilliporeSigma, St. Louis, MO, USA).
532 The membrane and cytosol proteins from LC lysate were isolated using Mem-PER Plus Kit
533 (78840, Thermo Fisher) in accordance with the manufacture's protocol. The protein
534 concentration of the lysate was determined using a Lowry protein assay (Bio-Rad, Hercules,
535 CA, USA). Protein samples (20 μg) were heated to 95°C for 5 min, separated by 12% sodium
536 dodecyl sulfate-polyacrylamide gel electrophoresis, and transferred to a polyvinylidene
537 fluoride membrane using a Transblot SD apparatus (Bio-Rad). After the blots had been washed
538 with tris-buffered saline containing Tween-20 (TBST, 10 mM Tris-HCl, 150 mM NaCl, 0.05%
539 Tween-20), the membranes were blocked with 2% BSA and 4% skim milk/TBST at RT for 1
540 h and incubated at 4°C overnight with primary antibodies, followed by an anti-rabbit IgG
541 horseradish peroxidase (HRP)-conjugated secondary antibody (1:5,000, 7074; Cell Signaling
542 Technology, Danvers, MA, USA) at RT for 1 h. The Western blot membrane was stripped the
543 primary and secondary antibodies and reprobed with the anti-β-actin antibody followed by the
544 anti-rabbit IgG HRP-conjugated secondary antibody. The following primary antibodies were
545 used for the blots: rabbit anti-α2A-AR (1:500; AAR020, alomone), rabbit anti-GAPDH
546 (1:1000; LF-PA0018, Abfrontier, Seoul, Korea), mouse anti-beta actin (1:2000, A5441,
547 MilliporeSigma) and rabbit anti-sodium potassium ATPase (1:1000; ab76020, Abchem)
548 (**Figure 3C, F and G**); rabbit anti-TH (1:1600; GTX113016, GeneTex, Irvine, CA, USA),
549 rabbit anti-MAO-A (1:6400; ab126751, Abcam), mouse anti-legumain (AEP) (1:400; sc-
550 133234, Santa Cruz), mouse anti-TAU-5 (1:1500, Santa Cruz Biotechnology, SC-58860) and
551 mouse anti-beta actin (1:12800, 66009-1-Ig, Proteintec, Rosemont, IL, USA) (**Figure 5A, D
552 and G**); rabbit anti-tau AEP-cleaved (N368) (1:5000, ABN1703, MilliporeSigma) and mouse

553 anti-beta actin (1:1000, A5441, MilliporeSigma) (**Figure 5G, I**). Western blot analysis was
554 performed by measuring band intensity with ImageJ 1.50i software (National Institutes of
555 Health, Bethesda, MD, USA).

556

557 **Quantitative real-time PCR**

558 cDNA was synthesized with Super Script II Reverse Transcriptase (18064, Invitrogen,
559 Carlsbad, CA, USA) with 1 mg of LC neuron RNA. Using a 7300 Gene Amp PCR system
560 (Applied Biosystems, Carlsbad), quantitative real-time PCR was run in Power SYBR Green
561 PCR master mix (4367656; Life Technologies, Carlsbad) under the following thermal cycling
562 conditions; an initial step of 94°C/5 min, followed by 40 cycles of a series of steps of 94°C/45
563 s, 61°C/45 s, 72°C/45 s and ended with a series of steps of 95°C/60 s, 60°C/1 min, 95°C/15 s,
564 60°C/15 s. The following primers were used: α2A (forward GGAATCATGGCTGTGGAGAT,
565 reverse CAGAAATCCCTTCCCTGTCA); α2C (forward TCATCGTTTTCACCGTGGTA,
566 reverse GCTCATTGGCCAGAGAAAAG); GIRK1 (forward
567 ACCCTGGTGGATCTCAAGTG, reverse GGCCACACAGGGAGTGTAGT); GRIK2
568 (forward CAACCTCAACGGGTTTGTCT, reverse ATCCTACCATGAAGGCGTTG);
569 GIRK3 (forward CGTCTCACCTCTCGTCATCA, reverse
570 CATCCACCAGGTACGAGCTT); GAPDH (forward CCAGAACATCATCCCTGCAT,
571 reverse GCATCGAAGGTGGAAGAGTG).

572

573 **Behavioral test**

574 The control mice as non-stress group and mice exposed to RS for 1 day, 3 days and 5 days as
575 1-day, 3-day and 5-day RS groups were tested on the Y maze apparatus, consisted of three
576 identical arms in a "Y" shape made of white acryl (35 cm in length, 5 cm in width, and 20 cm
577 in height) to assess working spatial memory. All tests were performed between 9 AM and
578 noon. Investigators were blinded to the group when performing experiments. Each mouse was
579 placed at the extremity of the "start arm" and left for a training session of 15 minutes, with one
580 of the 2 other arms closed with a white acrylic board (the closed arm was randomly chosen for
581 each mouse). Then, the mouse was brought back to its cage for 5 minutes, the maze was
582 cleaned, the closed arm was opened, and the mouse placed at the extremity of the start arm for
583 a 5-minute test session, under video tracking. The time spent and distance traveled in each arm
584 (start, familiar, and novel arms) were measured and analyzed with Smart 3.0 video tracking

585 software (Panlab, Harvard Apparatus, Holliston, MA, USA). Given their natural curiosity,
586 mice are expected to spend more time exploring the new arm.
587

588 **Drug application**

589 Atipamezole as a blocker of α2-AR and tertiapin-Q as a GIRK blocker were bath-applied at 5-
590 10 μM and 200 nM, respectively. Barbadin as an arrestin/AP2 blocker was added to the internal
591 solution at a final concentration of 100 μM (*Beautrait et al., 2017*). All chemicals except
592 tertiapin-Q were purchased from MilliporeSigma unless specified otherwise. Tertiapin-Q was
593 purchased from Tocris Bioscience (Bristol, UK).

594

595 **Statistical Analysis**

596 Statistical analysis was performed using STATISTICA10J (StatSoft Japan, Tokyo, Japan).
597 Numerical data were expressed as the mean ± SD. The statistical significance was assessed
598 using Student's *t*-test, one-way ANOVA followed by post hoc Fisher's PLSD and Wilk's
599 lambda. The significance level was set at 5% or less ($p < 0.05$). Statistical results are given as
600 a p value, unless $p < 0.001$. All the statistical data contained in this study are presented in
601 Table S1.

602

603 ## Acknowledgements

604 This research was funded by Japan Society for the Promotion of Science (26290006 and
605 21K06441 to Y.K.: 20K06926 and 23K06346 to H.T.). Y.K. was supported by Brain Pool
606 Program (NRF) funded by the Korean government (Ministry of Science and ICT). H.T. was
607 supported by Naito Foundation. This research was partly supported by the Basic Science
608 Research Program through the National Research Foundation of Korea grants (NRF-
609 2018R1A5A2024418 and NRF-2021R1A2C3003334 to S.B.O) funded by the Korean
610 government (Ministry of Science and ICT).
611

612 ## Author Contributions

613 YK, HT, and SBO conceived and designed the study. HT, DK, BGK, and TS performed
614 experiments. HT, DK, BGK, TS, TK, and YK analyzed data. YK, HT and SBO wrote the
615 manuscript.

Ethics

This study was conducted following the Helsinki Declaration, and carried out according to the ARRIVE guidelines. All experimental procedures were approved and performed in accordance with the relevant guidelines of the Ethical Guidelines Committee at Osaka University, Seoul National University and Kyushu University.

Data Availability

All data and/or analyses generated during the current study are available from the corresponding author upon request.

Competing Interests

The authors declare no competing financial or non-financial interests.

References

Aiken SP, Lampe BJ, Murphy PA, Brown BS. 1995. Reduction of spike frequency adaptation and blockade of M-current in rat CA1 pyramidal neurones by linopirdine (DuP 996), a neurotransmitter release enhancer. *Br J Pharmacol* **115**:1163-1168.

Aoki C, Go CG, Venkatesan C, Kurose H. 1994. Perikaryal and synaptic localization of α_{2A}-adrenergic receptor-like immunoreactivity. *Brain Res* **650**:181-204.

Arima J, Kubo C, Ishibashi H, Akaike N. 1998. α_2-Adrenoceptor-mediated potassium currents in acutely dissociated rat locus coeruleus neurones. *J Physiol* **508 (Pt 1)**:57-66.

Aziz Q, Thomas AM, Khambra T, Tinker A. 2012. Regulation of the ATP-sensitive potassium channel subunit, Kir6.2, by a Ca^{2+}-dependent protein kinase C. *J Biol Chem* **287**:6196-6207.

Barcomb K, Olah SS, Kennedy MJ, Ford CP. 2022. Properties and modulation of excitatory inputs to the locus coeruleus. *J Physiol* **600**:4897-4916.

Beattie EC, Carroll RC, Yu X, Morishita W, Yasuda H, von Zastrow M, Malenka RC. 2000. Regulation of AMPA receptor endocytosis by a signaling mechanism shared with LTD. *Nat Neurosci* **3**:1291-1300.

Beautrait A, Paradis JS, Zimmerman B, Giubilaro J, Nikolajev L, Armando S, Kobayashi H, Yamani L, Namkung Y, Heydenreich FM, Khoury E, Audet M, Roux PP, Veprintsev DB, Laporte SA, Bouvier M. 2017. A new inhibitor of the β-arrestin/AP2 endocytic complex reveals interplay between GPCR internalization and signalling. *Nat Commun* **8**:15054.

649 Bisht K, Sharma K, Tremblay ME. 2018. Chronic stress as a risk factor for Alzheimer's disease:
650 Roles of microglia-mediated synaptic remodeling, inflammation, and oxidative stress.
651 *Neurobiol Stress* **9**:9-21.

652 Bloom FE. 2006. Goodman & Gilman's the pharmacological basis of therapeutics (Brunton, L.
653 L. et al., eds). New York: McGraw-Hill; 2006: 283-304.

654 Borodovitsyna O, Joshi N, Chandler D. 2018. Persistent Stress-Induced Neuroplastic Changes
655 in the Locus Coeruleus/Norepinephrine System. *Neural Plast* **2018**:1892570.

656 Burke WJ, Kristal BS, Yu BP, Li SW, Lin TS. 1998. Norepinephrine transmitter metabolite
657 generates free radicals and activates mitochondrial permeability transition: a mechanism for
658 DOPEGAL-induced apoptosis. *Brain Res* **787**:328-332.

659 Burke WJ, Li SW, Schmitt CA, Xia P, Chung HD, Gillespie KN. 1999. Accumulation of 3,4-
660 dihydroxyphenylglycolaldehyde, the neurotoxic monoamine oxidase A metabolite of
661 norepinephrine, in locus ceruleus cell bodies in Alzheimer's disease: mechanism of neuron
662 death. *Brain Res* **816**:633-637.

663 Campos-Lira E, Kelly L, Seifi M, Jackson T, Giesecke T, Mutig K, Koshimizu TA, Hernandez
664 VS, Zhang L, Swinny JD. 2018. Dynamic modulation of mouse Locus coeruleus neurons
665 by vasopressin 1a and 1b receptors. *Front Neurosci* **12**:919.

666 Cao X, Wei Z, Gabriel GG, Li X, Mousseau DD. 2007. Calcium-sensitive regulation of
667 monoamine oxidase-A contributes to the production of peroxyradicals in hippocampal
668 cultures: implications for Alzheimer disease-related pathology. *BMC Neurosci* **8**:73.

669 Chen Y, Chen T, Hou R. 2022. Locus coeruleus in the pathogenesis of Alzheimer's disease: A
670 systematic review. *Alzheimers Dement (N Y)* **8**:e12257.

671 Chu X, Zhou Y, Hu Z, Lou J, Song W, Li J, Liang X, Chen C, Wang S, Yang B, Chen L, Zhang
672 X, Song J, Dong Y, Chen S, He L, Xie Q, Chen X, Li W. 2016. 24-hour-restraint stress
673 induces long-term depressive-like phenotypes in mice. *Sci Rep* **6**:32935.

674 Costa VM, Carvalho, F., Bastos, M.L., Carvalho, R.A., Carvalho, M., Remião, F. 2012.
675 Adrenaline and noradrenaline: Partners and actors in the same play. (Contreras, C.M.,eds).
676 In: Neuroscience-Dealing with Frontiers. InTech, 2012: 1-44.

677 Cottingham C, Chen Y, Jiao K, Wang Q. 2011. The antidepressant desipramine is an arrestin-
678 biased ligand at the α_{2A}-adrenergic receptor driving receptor down-regulation in vitro and
679 in vivo. *J Biol Chem* **286**:36063-36075.

680 Counts SE, Mufson EJ. 2010. Noradrenaline activation of neurotrophic pathways protects
681 against neuronal amyloid toxicity. *J Neurochem* **113**:649-660.

682 DeGraff JL, Gagnon AW, Benovic JL, Orsini MJ. 1999. Role of arrestins in endocytosis and
683 signaling of α_2-adrenergic receptor subtypes. *J Biol Chem* **274**:11253-11259.

684 Eisenhofer G, Kopin IJ, Goldstein DS. 2004. Catecholamine metabolism: a contemporary view
685 with implications for physiology and medicine. *Pharmacol Rev* **56**:331-349.

686 Eisenhofer G, Esler MD, Meredith IT, Dart A, Cannon RO, 3rd, Quyyumi AA, Lambert G,
687 Chin J, Jennings GL, Goldstein DS. 1992. Sympathetic nervous function in human heart as
688 assessed by cardiac spillovers of dihydroxyphenylglycol and norepinephrine. *Circulation*
689 **85**:1775-1785.

690 Feng J, Zhang C, Lischinsky JE, Jing M, Zhou J, Wang H, Zhang Y, Dong A, Wu Z, Wu H,
691 Chen W, Zhang P, Zou J, Hires SA, Zhu JJ, Cui G, Lin D, Du J, Li Y. 2019. A Genetically
692 Encoded Fluorescent Sensor for Rapid and Specific In Vivo Detection of Norepinephrine.
693 *Neuron* **102**:745-761 e748.

694 Flugge G. 1996. Alterations in the central nervous α2-adrenoceptor system under chronic
695 psychosocial stress. *Neuroscience* **75**:187-196.

696 Goedert M, Spillantini MG, Potier MC, Ulrich J, Crowther RA. 1989. Cloning and sequencing
697 of the cDNA encoding an isoform of microtubule-associated protein tau containing four
698 tandem repeats: differential expression of tau protein mRNAs in human brain. *EMBO J*
699 **8**:393-399.

700 Goldstein DS. 2021. The catecholaldehyde hypothesis for the pathogenesis of
701 catecholaminergic neurodegeneration: What we know and what we do not know. *Int J Mol*
702 *Sci* **22**.

703 Gray M, Bingham B, Viau V. 2010. A comparison of two repeated restraint stress paradigms
704 on hypothalamic-pituitary-adrenal axis habituation, gonadal status and central neuropeptide
705 expression in adult male rats. *J Neuroendocrinol* **22**:92-101.

706 Hettie KS, Glass TE. 2014. Coumarin-3-aldehyde as a scaffold for the design of tunable PET-
707 modulated fluorescent sensors for neurotransmitters. *Chemistry* **20**:17488-17499.

708 Huang HP, Wang SR, Yao W, Zhang C, Zhou Y, Chen XW, Zhang B, Xiong W, Wang LY, Zheng
709 LH, Landry M, Hokfelt T, Xu ZQ, Zhou Z. 2007. Long latency of evoked quantal transmitter
710 release from somata of locus coeruleus neurons in rat pontine slices. *Proc Natl Acad Sci U*
711 *S A* **104**:1401-1406.

712 Itoi K, Sugimoto N. 2010. The brainstem noradrenergic systems in stress, anxiety and
713 depression. *J Neuroendocrinol* **22**:355-361.

714 Jedema HP, Gold SJ, Gonzalez-Burgos G, Sved AF, Tobe BJ, Wensel T, Grace AA. 2008.
715 Chronic cold exposure increases RGS7 expression and decreases α2-autoreceptor-mediated
716 inhibition of noradrenergic locus coeruleus neurons. *Eur J Neurosci* **27**:2433-2443.

717 Kang SS, Liu X, Ahn EH, Xiang J, Manfredsson FP, Yang X, Luo HR, Liles LC, Weinshenker
718 D, Ye K. 2020. Norepinephrine metabolite DOPEGAL activates AEP and pathological Tau
719 aggregation in locus coeruleus. *J Clin Invest* **130**:422-437.

720 Kielbasa W, Pan A, Pereira A. 2015. A pharmacokinetic/pharmacodynamic investigation:
721 assessment of edivoxetine and atomoxetine on systemic and central 3,4-
722 dihydroxyphenylglycol, a biochemical marker for norepinephrine transporter inhibition. *Eur*
723 *Neuropsychopharmacol* **25**:377-385.

724 Kitayama IT, Otani M, Murase S. 2004. Contribution of the stress-induced degeneration of the
725 locus coeruleus noradrenergic neurons to the pathophysiology of depression: a study on an
726 animal model. *Acta Neuropsychiatr* **16**:190-199.

727 Koenig JH, Ikeda K. 1996. Synaptic vesicles have two distinct recycling pathways. *J Cell Biol*
728 **135**:797-808.

729 Leistner C, Menke A. 2020. Hypothalamic-pituitary-adrenal axis and stress. *Handb Clin Neurol*
730 **175**:55-64.

731 Mao L, Han Y, Zhang QW, Tian Y. 2023. Two-photon fluorescence imaging and specifically
732 biosensing of norepinephrine on a 100-ms timescale. *Nat Commun* **14**:1419.

733 Mather M, Harley CW. 2016. The locus coeruleus: essential for maintaining cognitive function
734 and the aging brain. *Trends Cogn Sci* **20**:214-226.

735 McCall JG, Al-Hasani R, Siuda ER, Hong DY, Norris AJ, Ford CP, Bruchas MR. 2015. CRH
736 Engagement of the Locus Coeruleus Noradrenergic System Mediates Stress-Induced
737 Anxiety. *Neuron* **87**:605-620.

738 Mitchell NC, Bowman MA, Gould GG, Koek W, Daws LC. 2017. Ontogeny of norepinephrine
739 rransporter expression and antidepressant-like response to desipramine in wild-type and
740 serotonin transporter mutant mice. *J Pharmacol Exp Ther* **360**:84-94.

741 Pierce KL, Lefkowitz RJ. 2001. Classical and new roles of β-arrestins in the regulation of G-
742 protein-coupled receptors. *Nat Rev Neurosci* **2**:727-733.

743 Potter LT, Axelrod J. 1963. Properties of norepinephrine storage particles of the rat heart. *J*
744 *Pharmacol Exp Ther* **142**:299-305.

745 Ross JA, McGonigle P, Van Bockstaele EJ. 2015. Locus coeruleus, norepinephrine and Aβ
746 peptides in Alzheimer's disease. *Neurobiol Stress* **2**:73-84.

747 Sakaguchi T, Nakamura S. 1990. Duration-dependent effects of repeated restraint stress on
748 cortical projections of locus coeruleus neurons. *Neurosci Lett* **118**:193-196.

749 Sanders JD, Happe HK, Bylund DB, Murrin LC. 2005. Development of the norepinephrine
750 transporter in the rat CNS. *Neuroscience* **130**:107-117.

751 Sarmento MJ, Coutinho A, Fedorov A, Prieto M, Fernandes F. 2014. Ca^{2+} induces $PI(4,5)P_2$
752 clusters on lipid bilayers at physiological $PI(4,5)P_2$ and Ca^{2+} concentrations. *Biochim*
753 *Biophys Acta* **1838**:822-830.

754 Stone LS, Broberger C, Vulchanova L, Wilcox GL, Hokfelt T, Riedl MS, Elde R. 1998.
755 Differential distribution of α2A and α2C adrenergic receptor immunoreactivity in the rat
756 spinal cord. *J Neurosci* **18**:5928-5937.

757 Sugama S, Sekiyama K, Kodama T, Takamatsu Y, Takenouchi T, Hashimoto M, Bruno C,
758 Kakinuma Y. 2016. Chronic restraint stress triggers dopaminergic and noradrenergic
759 neurodegeneration: Possible role of chronic stress in the onset of Parkinson's disease. *Brain*
760 *Behav Immun* **51**:39-46.

761 Takahashi N, Miner LL, Sora I, Ujike H, Revay RS, Kostic V, Jackson-Lewis V, Przedborski
762 S, Uhl GR. 1997. VMAT2 knockout mice: heterozygotes display reduced amphetamine-
763 conditioned reward, enhanced amphetamine locomotion, and enhanced MPTP toxicity. *Proc*
764 *Natl Acad Sci U S A* **94**:9938-9943.

765 Takei K, Mundigl O, Daniell L, De Camilli P. 1996. The synaptic vesicle cycle: a single vesicle
766 budding step involving clathrin and dynamin. *J Cell Biol* **133**:1237-1250.

767 Tan M, Walwyn WM, Evans CJ, Xie CW. 2009. p38 MAPK and β-arrestin 2 mediate functional
768 interactions between endogenous micro-opioid and α2A-adrenergic receptors in neurons. *J*
769 *Biol Chem* **284**:6270-6281.

770 Taraviras S, Olli-Lahdesmaki T, Lymperopoulos A, Charitonidou D, Mavroidis M, Kallio J,
771 Scheinin M, Flordellis C. 2002. Subtype-specific neuronal differentiation of PC12 cells
772 transfected with α2-adrenergic receptors. *Eur J Cell Biol* **81**:363-374.

773 Torres GE, Gainetdinov RR, Caron MG. 2003. Plasma membrane monoamine transporters:
774 structure, regulation and function. *Nat Rev Neurosci* **4**:13-25.

775 Toyoda H, Won J, Kim W, Kim H, Davy O, Saito M, Kim D, Tanaka T, Kang Y, Oh SB. 2022.
776 The Nature of Noradrenergic Volume Transmission From Locus Coeruleus to Brainstem
777 Mesencephalic Trigeminal Sensory Neurons. *Front Cell Neurosci* **16**:841239.

778 Valentino RJ, Foote SL. 1988. Corticotropin-releasing hormone increases tonic but not
779 sensory-evoked activity of noradrenergic locus coeruleus neurons in unanesthetized rats. *J*
780 *Neurosci* **8**:1016-1025.

781 Valentino RJ, Foote SL, Aston-Jones G. 1983. Corticotropin-releasing factor activates
782 noradrenergic neurons of the locus coeruleus. *Brain Res* **270**:363-367.

783 Valentino RJ, Rudoy C, Saunders A, Liu XB, Van Bockstaele EJ. 2001. Corticotropin-releasing
784 factor is preferentially colocalized with excitatory rather than inhibitory amino acids in axon
785 terminals in the peri-locus coeruleus region. *Neuroscience* **106**:375-384.

786 Williams JT, Henderson G, North RA. 1985. Characterization of α_2-adrenoceptors which
787 increase potassium conductance in rat locus coeruleus neurones. *Neuroscience* **14**:95-101.

788 Zaccor NW, Sumner CJ, Snyder SH. 2020. The nonselective cation channel TRPV4 inhibits
789 angiotensin II receptors. *J Biol Chem* **295**:9986-9997.

790 Zhang Y, Woodruff M, Zhang Y, Miao J, Hanley G, Stuart C, Zeng X, Prabhakar S, Moorman
791 J, Zhao B, Yin D. 2008. Toll-like receptor 4 mediates chronic restraint stress-induced
792 immune suppression. *J Neuroimmunol* **194**:115-122.

793 Zhang Z, Song M, Liu X, Kang SS, Kwon IS, Duong DM, Seyfried NT, Hu WT, Liu Z, Wang
794 JZ, Cheng L, Sun YE, Yu SP, Levey AI, Ye K. 2014. Cleavage of tau by asparagine
795 endopeptidase mediates the neurofibrillary pathology in Alzheimer's disease. *Nat Med*
796 **20**:1254-1262.

797

798

799 ## Figure legends

800 **Figure 1. Atipamezole abolishes spike-frequency adaptation and blocks NA-induced**
801 **GIRK-I in LC neurons.**

802 (**A, B**) Sample traces of spike trains induced in an LC neuron by injection of current pulses at
803 75 and 100 pA. Note the spike-frequency adaptation and pulse-afterhyperpolarization (pulse-
804 AHP).

805 (**C**) Plotting of the cumulative spike numbers vs the elapsed time from the onset of the current
806 pulses every 50 ms at 75 pA (blue circles) or 100 pA (red circles) (n = 7). Two-way RM
807 ANOVA, $*p < 0.001$. The saturation level (***a***) and the half saturation constant (***b***) were
808 measured by fitting the saturation function defined as y = (***a*** * x) / (***b*** + x) to the data points.
809 The values of ***a*** at 75 and 100 pA current pulses were 44.6 ± 16.2 and 52.5 ± 12.3, respectively
810 (paired t-test, p = 0.010). The values of ***b*** at 75 and 100 pA current pulses were 2.1 ± 0.7 and
811 2.1 ± 0.4, respectively (paired t-test, p = 0.823).

812 (**D, E**) Sample traces of spike trains induced in an LC neuron evoked by current pulses at 100
813 pA under control condition and after application of 10 μM atipamezole. Note that atipamezole
814 suppresses spike-frequency adaptation and pulse-AHP (blue and red stars).

815 (**F**) Plotting of the cumulative spike numbers vs the elapsed time during the current pulses
816 every 50 ms before and after application of atipamezole (blue and red circles, respectively) (n
817 = 10). Two-way RM ANOVA, $*p < 0.001$.

818 (**G**) Plotting of ***a*** against ***b***, which were measured by fitting the saturation function to the data
819 points in **F**. Both the values of ***a*** and ***b*** obtained by curve fitting to the data points after
820 application of atipamezole (open and filled red circles) were significantly shifted to larger
821 values than those obtained under control condition (open and filled blue circles) (paired t-test,
822 ***a*** and ***b***, $^{‡}p$ = 0.003 and $^{‡}p$ = 0.002, respectively), and there was a significant difference in the
823 relationship between ***a*** and ***b*** (Wilk's lambda, $^{§}p$ = 0.002) (n = 10).

824 (**H**) Top, Voltage command pulse. Lower panel, Superimposed current traces obtained under
825 control condition (1), after application of 100 μM NA (2), and after application of 10 μM
826 atipamezole (Atip) in addition to NA (3). The amplitudes of inward and outward components
827 in NA-induced GIRK-I were –70 ± 22 and 36 ± 11 pA, respectively (paired t-test, $^{‡}p$ = 0.005,
828 n = 6).

829 (**I**) A graph showing the effects of atipamezole on amplitudes of the inward and outward
830 components of NA-induced GIRK-I at –130 mV and –60 mV, obtained by subtraction of
831 currents recorded under control condition from those recorded after application of NA (2–1)

832 and from those recorded after application of NA and atipamezole (3–1). Inward component,
833 paired *t*-test, $^{\ddagger}p < 0.001$; outward component, paired *t*-test, $^{\ddagger}p < 0.001$ ($n = 6$).
834
835 **Figure 2. Ca^{2+}-dependent rundown of NA-induced GIRK-I and its suppression by**
836 **barbadin.**
837 (**A**) Upper panel, Ramp command pulse. Lower panel, Superimposed current traces obtained
838 under control condition (1) and after application of 100 μM NA for 5 min (2).
839 (**B**) Upper panel, A combined command pulse applied every minute; five trains of 20 positive
840 pulses (5 ms duration to 0 mV at 20 Hz) at an interval of 2 s in the presence of extracellular 30
841 mM TEA and intracellular 0.2 mM EGTA, which were followed by the ramp pulse after an
842 interval of 25 s. Lower panel, representative Ca^{2+} currents in response to positive pulses in the
843 presence of NA and 30 mM TEA.
844 (**C**) Upper panel, Ramp command pulse. Lower panel, Superimposed current traces obtained
845 after application of NA for 5 min (2) and in response to application of the 20th combined pulse
846 in the presence of NA and TEA (3).
847 (**D**) The I-V relationship of NA-induced GIRK-I obtained by subtraction of currents recorded
848 under control condition from that recorded after application of NA for 5 min (red trace, 2–1)
849 and that obtained by subtraction of the control current from that recorded in response to
850 application of the 20th combined pulse in the presence of NA and TEA (blue trace, 3–1).
851 (**E**) Plotting of amplitudes of inward components at –130 mV (blue circles) and outward
852 components at –60 mV (red circles) against time.
853 (**F**) Plotting of normalized amplitudes of inward components at –130 mV and outward
854 components at –60 mV before and 20 min after application of positive pulse trains in the
855 presence of NA and TEA. The amplitudes of inward components at –130 mV and those of
856 outward components at –60 mV were normalized by those recorded in the presence of NA
857 before applying positive pulse trains. Inward component, paired *t*-test, $^{\ddagger}p < 0.001$; outward
858 component, paired *t*-test, $^{\ddagger}p < 0.001$ ($n = 8$).
859 (**G**) Upper panel, Ramp command pulse. Lower panel, Superimposed current traces obtained
860 under control condition (1) and after application of 100 μM NA for 5 min (2) in LC neurons
861 dialyzed with 100 μM barbadin (β-arrestin/AP2 blocker).
862 (**H**) Upper panel, A combined command pulse applied every minute; five trains of 20 positive
863 pulses (5 ms duration to 0 mV at 20 Hz) at an inter-train interval of 2 s in the presence of
864 extracellular 30 mM TEA and intracellular 0.2 mM EGTA, which were followed by the ramp

865 pulse after an interval of 25 s. Lower panel, Superimposed current traces obtained after
866 application of NA for 5 min (2) and in response to application of the 20th combined pulse in
867 the presence of NA and TEA (3) in LC neurons dialyzed with barbadin.
868 (**I**) The I-V relationship of NA-induced GIRK-I obtained by subtraction of currents recorded
869 under control condition from that recorded after application of NA for 5 min (red trace, 2–1)
870 and that obtained by subtraction of the control current from that recorded in response to
871 application of the 20th combined pulse in the presence of NA and TEA (blue trace, 3–1).
872 (**J**) Plotting of normalized amplitudes (left vertical axis) of inward components at –130 mV
873 (filled blue circles) and outward components at –60 mV (filled red circles) against time ($n = 8$).
874 Amplitudes of GIRK-I were normalized to the values obtained before applying pulse trains.
875 Right vertical axis refers to the original amplitudes. Open blue and red circles represent the
876 normalized amplitudes of GIRK-I shown in **E**.
877 (**K**) Plotting of normalized amplitudes of inward components at –130 mV and outward
878 components at –60 mV before and 20 min after application of positive pulse trains in the
879 presence of NA and TEA ($n = 8$). The amplitudes of inward components at –130 mV and those
880 of outward components at –60 mV were normalized to those recorded in the presence of NA
881 before applying positive pulse trains. Open light pink circles represent results obtained under
882 the control condition in **F**. Inward component, unpaired *t*-test, $*p < 0.001$; outward component,
883 unpaired *t*-test, $*p < 0.001$.
884
885 **Figure 3. RS reduces expression of α2A-ARs in LC Neurons.**
886 (**A, B**) Confocal images of LC neurons showing immunoreactivities for TH and α2A-ARs,
887 together with a merged one in non-stress and 3-day RS mice. Arrowheads indicate the
888 membrane regions of TH-positive neurons, along which α2A-ARs were differentially
889 expressed between the control and the RS mice. Asterisks indicate LC neurons.
890 (**C**) Western blotting analyses showing the expression of α2A-ARs in non-stress and 3-day RS
891 mice ($n = 6$ and 7, respectively). Unpaired *t*-test, $^{\dagger}p < 0.001$.
892 (**D, E**) Confocal images of LC neurons in non-stress and RS mice. Upper panels from left to
893 right showing the respective immunoreactivity for TH, α2A-ARs (with rabbit anti-α2A-AR)
894 and Na^+-K^+-pump and an enlarged image of the region enclosed with a rectangle (arrowheads)
895 in its immediate left panel. Lower panels from left to right showing the merged image of TH
896 and α2A-ARs, that of TH, α2A-ARs and Na^+-K^+-pump, that of α2A-ARs and Na^+-K^+-pump
897 and an enlarged image of the region enclosed with a rectangle in its immediate left panel.

898 (**F, G**) Western blotting analyses showing expressions of α2A-ARs and Na^+-K^+-pump in
899 membrane fraction and those of α2A-ARs and β-actin in cytosol fraction in non-stress and 5-
900 day RS mice (n = 3 and 3 samples, respectively). Each sample represents the analysis result in
901 the LC tissues obtained from 2-3 mice. Membrane; unpaired t-test, $^{\dagger}p = 0.016$. Cytosol;
902 unpaired t-test, $^{\dagger}p = 0.083$.
903
904 **Figure 4. RS reduces NA-induced GIRK-I in LC neurons.**
905 (**A-E**) Representative traces of NA-induced GIRK-I obtained from LC neurons in non-stress
906 and 1-day, 2-day, 3-day, and 5-day RS mice.
907 (**F, G**) Amplitudes of inward and outward components of NA-induced GIRK-I obtained from
908 LC neurons in non-stress and 1-day, 2-day, 3-day, and 5-day RS mice (n = 8, 7, 5, 6 and 8,
909 respectively) decreased with the increase in the period of RS, in a way that can be described by
910 a saturation function (red interrupted lines). The saturation level (***a*** + ***b***) and the half saturation
911 constant (***c***) were determined by fitting the saturation function, defined as y = ***a*** + (***b**** x) / (***c*** +
912 x), to the data points. The values of ***a***, ***b*** and ***c*** for the inward component of GIRK-I were –151.1,
913 108, and 0.9, respectively, and those for the outward component of GIRK-I were 81.1, –67,
914 and 1.6, respectively. Inward component: one-way ANOVA, $p < 0.001$, post hoc fisher's
915 PLSD, 1-day; $^{\#}p < 0.001$ vs Non-stress and $^{*}p < 0.05$ vs 3-day and 5-day, 2-day; $^{\#}p < 0.001$ vs
916 Non-stress, 3-day; $^{\#}p < 0.001$ vs Non-stress, 5-day; $^{\#}p < 0.001$ vs Non-stress. Outward
917 component: one-way ANOVA, $p < 0.001$, post hoc fisher's PLSD, 1-day; $p = 0.004$ vs Non-
918 stress and $^{*}p < 0.05$ vs 3-day and 5-day, 2-day; $p = 0.015$ vs Non-stress, 3-day; $p < 0.001$ vs
919 Non-stress, 5-day; $p < 0.001$ vs Non-stress.
920 (**H**) Relative expressions of α2A and α2C mRNAs, normalized to GAPDH in LC neurons (n =
921 5). Paired t-test, $^{\ddagger}p = 0.014$.
922 (**I**) Relative expressions of GIRK1, GIRK2, and GIRK3 mRNAs, normalized to GAPDH in
923 LC neurons (n = 5). One-way RM ANOVA, $p < 0.001$, post hoc fisher's PLSD; $^{*}p = 0.008$
924 for GIRK1 vs GIRK2, $^{*}p < 0.001$ for GIRK1 vs GIRK3, $^{*}p = 0.008$ for GIRK2 vs GIRK3.
925 (**J, K**) Relative expressions of α2A and GIRK1 mRNAs, respectively, normalized to GAPDH
926 in LC neurons in non-stress mice (n = 8), and 3-day RS mice (n = 6). α2A-AR: unpaired t-test,
927 $^{\dagger}p = 0.020$; GIRK1: unpaired t-test, $^{\dagger}p = 0.013$.
928 (**L**) Normalized relative expressions of GIRK2 mRNA in LC neurons in non-stress mice (n =
929 8) and 3-day RS mice (n = 6), normalized to the ratio of the mean value of the relative

930 expressions of GIRK1 mRNA to that of GIRK2 mRNA in LC neurons in non-stress mice (**I**).
931 Unpaired *t*-test, $^{\dagger}p = 0.037$.
932
933 **Figure 5. Expressions of TH, MAO-A, DBH, AEP and tau proteins in LC neurons.**
934 (**A**) Western blotting of TH and MAO-A in LC neurons obtained from non-stress and 5-day
935 RS mice.
936 (**B, C**) Western blot analysis revealing no significant change in TH expression ($n = 10$ samples)
937 but a significant increase in MAO-A expression ($n = 6$ samples) in 5-day RS group compared
938 to non-stress group. Unpaired *t*-test, $^{\dagger}p = 0.029$.
939 (**D**) Western blotting of pro-AEP and active AEP in LC neurons obtained from non-stress and
940 5-day RS mice.
941 (**E, F**) Western blot analysis revealing significant increases in pro-AEP and active AEP ($n = 6$
942 and $n = 6$ samples, respectively) in 5-day RS group compared to non-stress group. Unpaired
943 *t*-test, $^{\dagger}p = 0.034$ (**E**) and $^{\dagger}p = 0.047$ (**F**).
944 (**G**) Western blotting of tau and tau N368 fragment in LC neurons obtained from non-stress
945 and 5-day RS mice. Unpaired *t*-test, $^{\dagger}p = 0.025$.
946 (**H, I**) Western blot analyses revealing a significant increase in tau and tau N368 fragment in
947 LC neurons ($n = 8$, and $n = 6$, respectively) in 5-day RS group compared to non-stress group.
948 Each sample represents the analysis result in the LC tissues obtained from 2-3 mice. Unpaired
949 *t*-test, $^{\dagger}p < 0.05$.
950
951 **Figure 6. Presumed cellular mechanisms for the degeneration of LC by stress.**
952 (**A, B**) Differential free concentrations of NA to be metabolized by MAO-A into DOPEGAL
953 between control and stress conditions: Under the control condition (**A**), NA in the cytosol is
954 mostly taken up into the cytoplasmic vesicles by VMAT2 (thick arrow 3), rather than being
955 directly metabolized by MAO-A into DOPEGAL (thin interrupted arrow). Vesicular NA is
956 released from cell bodies as autocrine following $[Ca^{2+}]_i$ increases caused by action potentials,
957 and the released NA activates α2A-AR-coupled GIRK channels, causing autoinhibition.
958 Subsequently, the autocrine released NA is slowly taken up into the cytosol of LC neurons by
959 NAT after dissociation from α2A-ARs. Under the stress condition (**B**), an activation of CRF
960 receptors in LC neurons by stress inhibits leak K^+ channels and increases firing activities in LC
961 neurons, subsequently causing a larger $[Ca^{2+}]_i$ increase together with Ca^{2+}-induced Ca^{2+} release
962 (CICR). Impairment of autoinhibiton due to Ca^{2+} dependent internalization of α2A-ARs-

963 coupled GIRK channels leads to the persistent excitation in LC neurons, which enhances
964 autocrine release of NA (thick arrow 1). Subsequently, the excessively autocrine released NA
965 is taken up directly and rapidly by NAT into the cytosol without binding to α2A-ARs (thick
966 arrow 2). Such a facilitation of re-uptake of NA by NAT would increase active NA storage into
967 cytoplasmic vesicles by VMAT2 (thick arrow 3), while the rate of NA leakage from
968 cytoplasmic vesicles would also increase (arrow 4) due to a dynamic equilibrium in
969 cytoplasmic vesicles between active NA storage into cytoplasmic vesicles and passive NA
970 leakage from cytoplasmic vesicles. Subsequently, such an increase in the rate of NA leakage
971 would result in an increase in a MAO-A metabolite, DOPEGAL and AEP, leading to a
972 production of cleaved tau N368 fragment and an impairment of learning/memory.

Figure 1

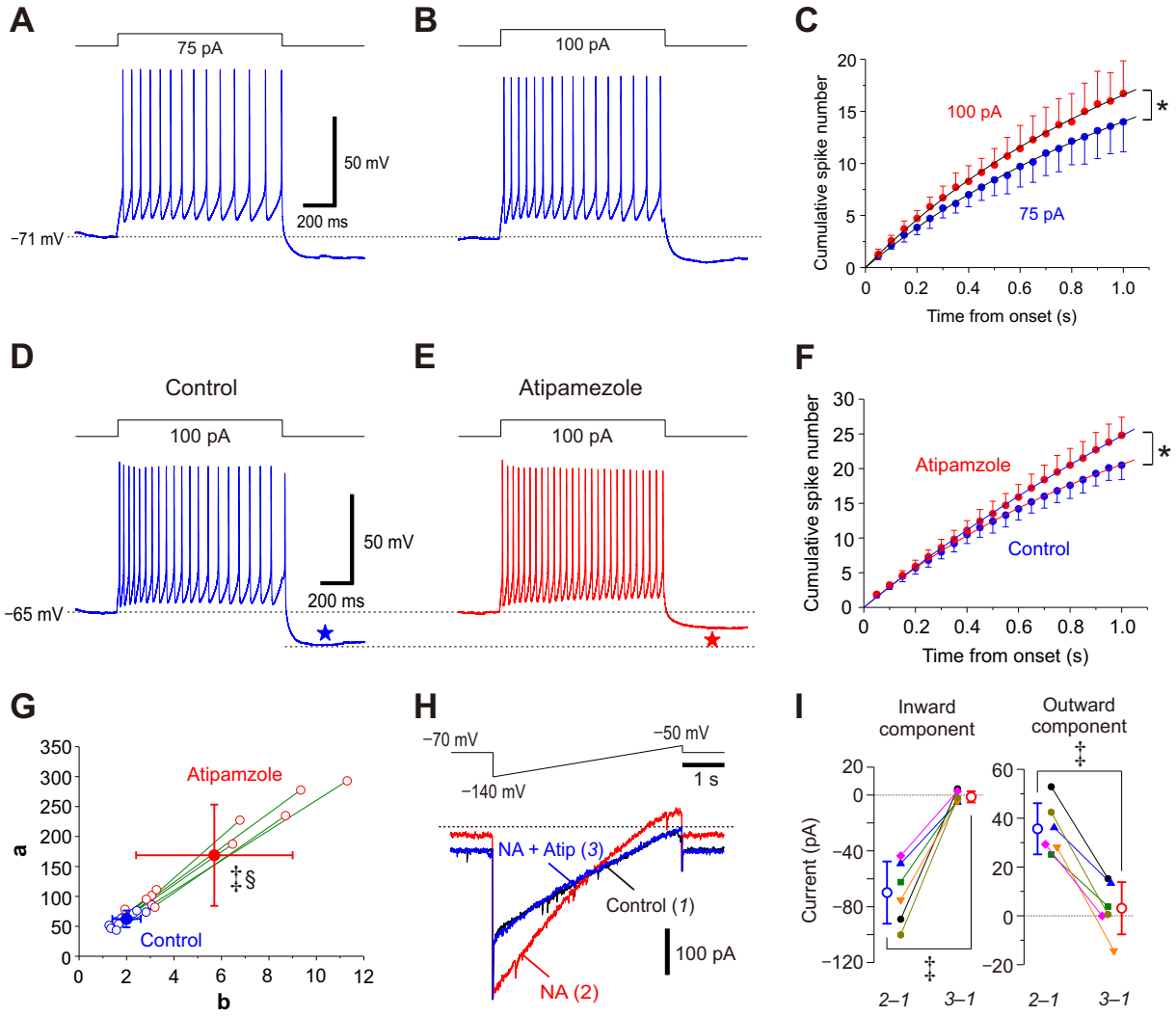
A
75 pA
50 mV
200 ms
−71 mV
B
100 pA
C
Cumulative spike number
100 pA
75 pA
*
Time from onset (s)
D
Control
100 pA
50 mV
200 ms
−65 mV
E
Atipamezole
100 pA
F
Cumulative spike number
Atipamzole
Control
*
Time from onset (s)
G
Atipamzole
Control
a
b
‡§
H
−70 mV
−50 mV
−140 mV
1 s
NA + Atip (3)
Control (1)
100 pA
NA (2)
I
Inward component
Outward component
Current (pA)
2–1
3–1
2–1
3–1

Figure 2

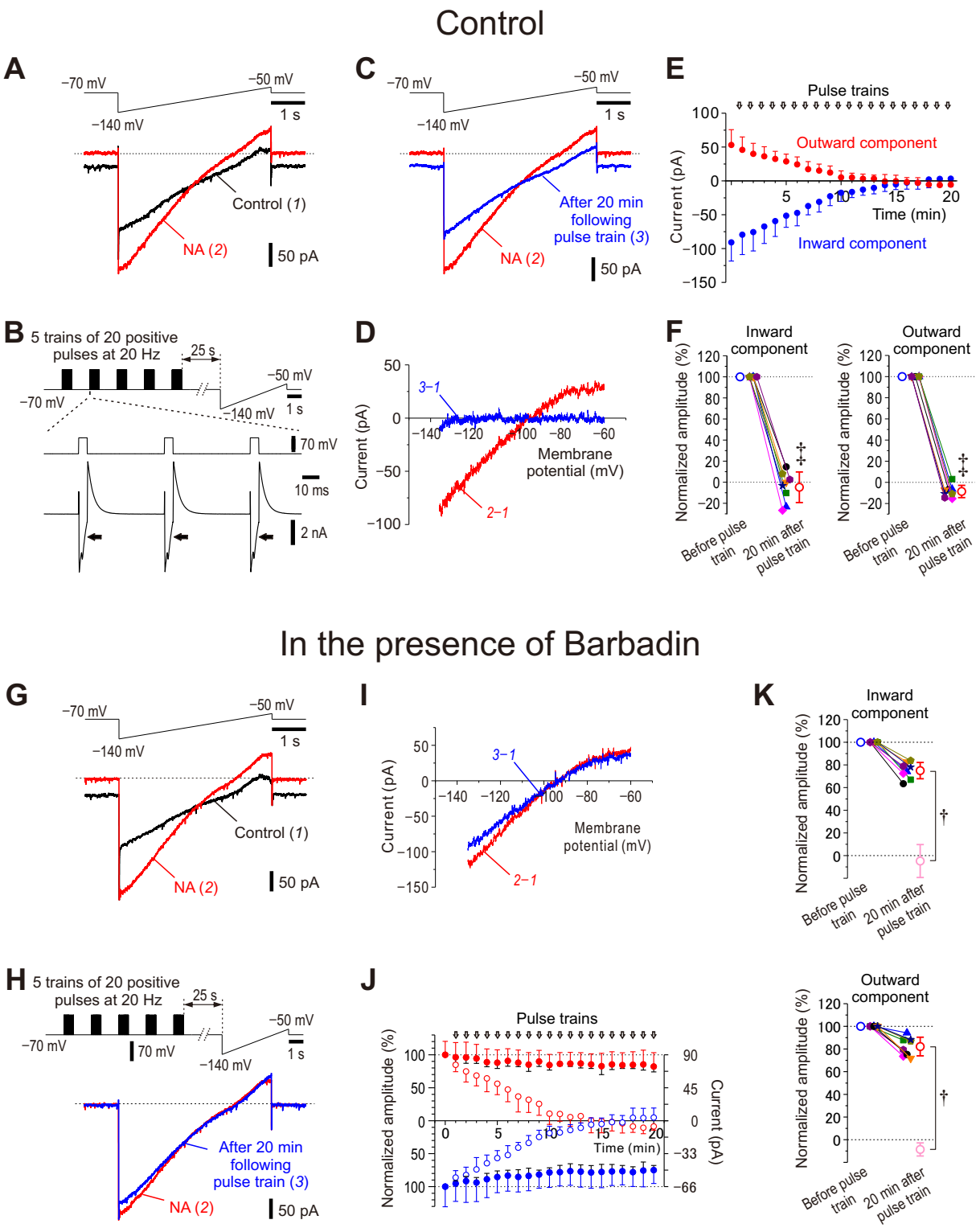
Control
A
−70 mV
−50 mV
−140 mV
1 s
Control (1)
NA (2)
50 pA
C
After 20 min following pulse train (3)
E
Pulse trains
Outward component
Inward component
Current (pA)
Time (min)
B
5 trains of 20 positive pulses at 20 Hz
25 s
70 mV
10 ms
2 nA
D
3−1
2−1
Membrane potential (mV)
F
Inward component
Outward component
Normalized amplitude (%)
Before pulse train
20 min after pulse train
In the presence of Barbadin
G
I
K
H
J

Figure 3

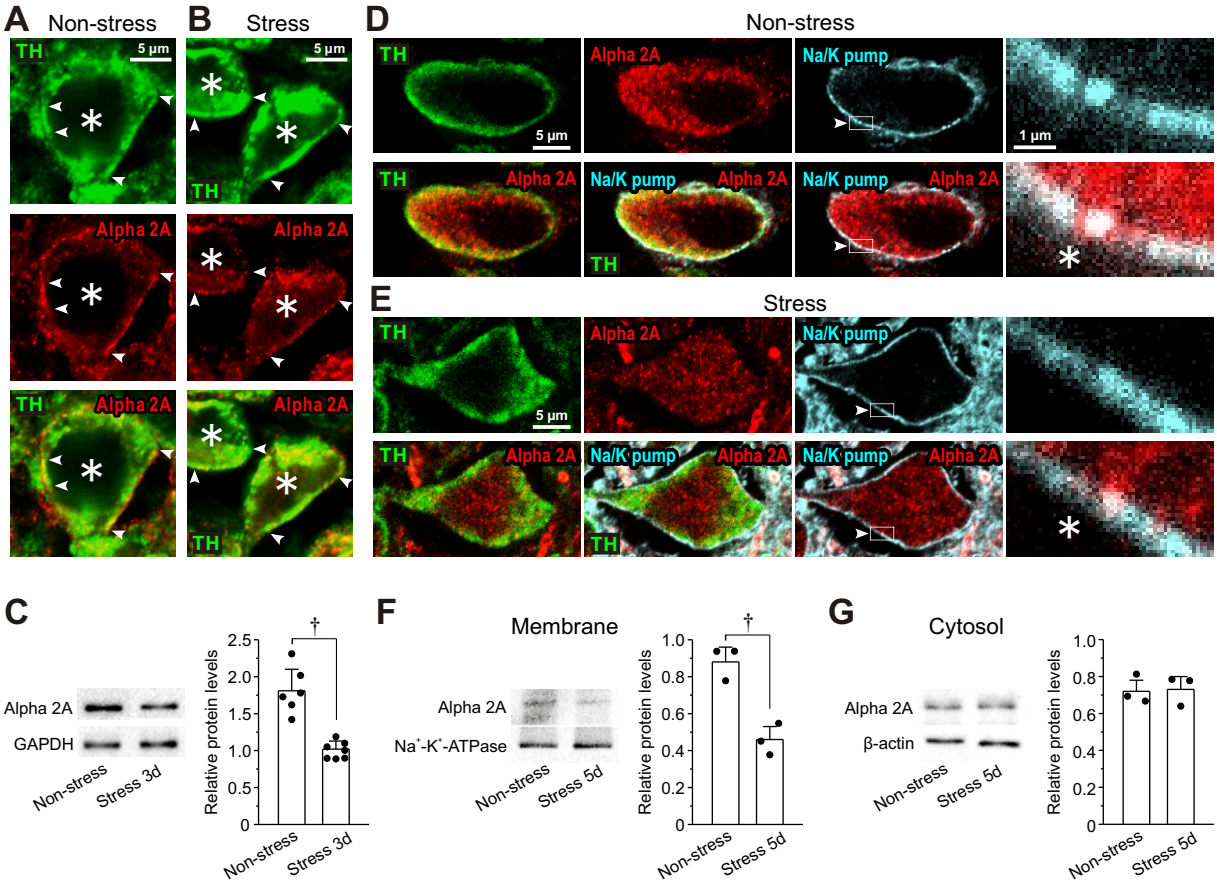
A
Non-stress
B
Stress
TH
5 µm
Alpha 2A
D
Non-stress
Na/K pump
1 µm
E
Stress
C
Alpha 2A
GAPDH
Non-stress
Stress 3d
Relative protein levels
F
Membrane
Na+-K+-ATPase
Stress 5d
G
Cytosol
β-actin

Figure 4

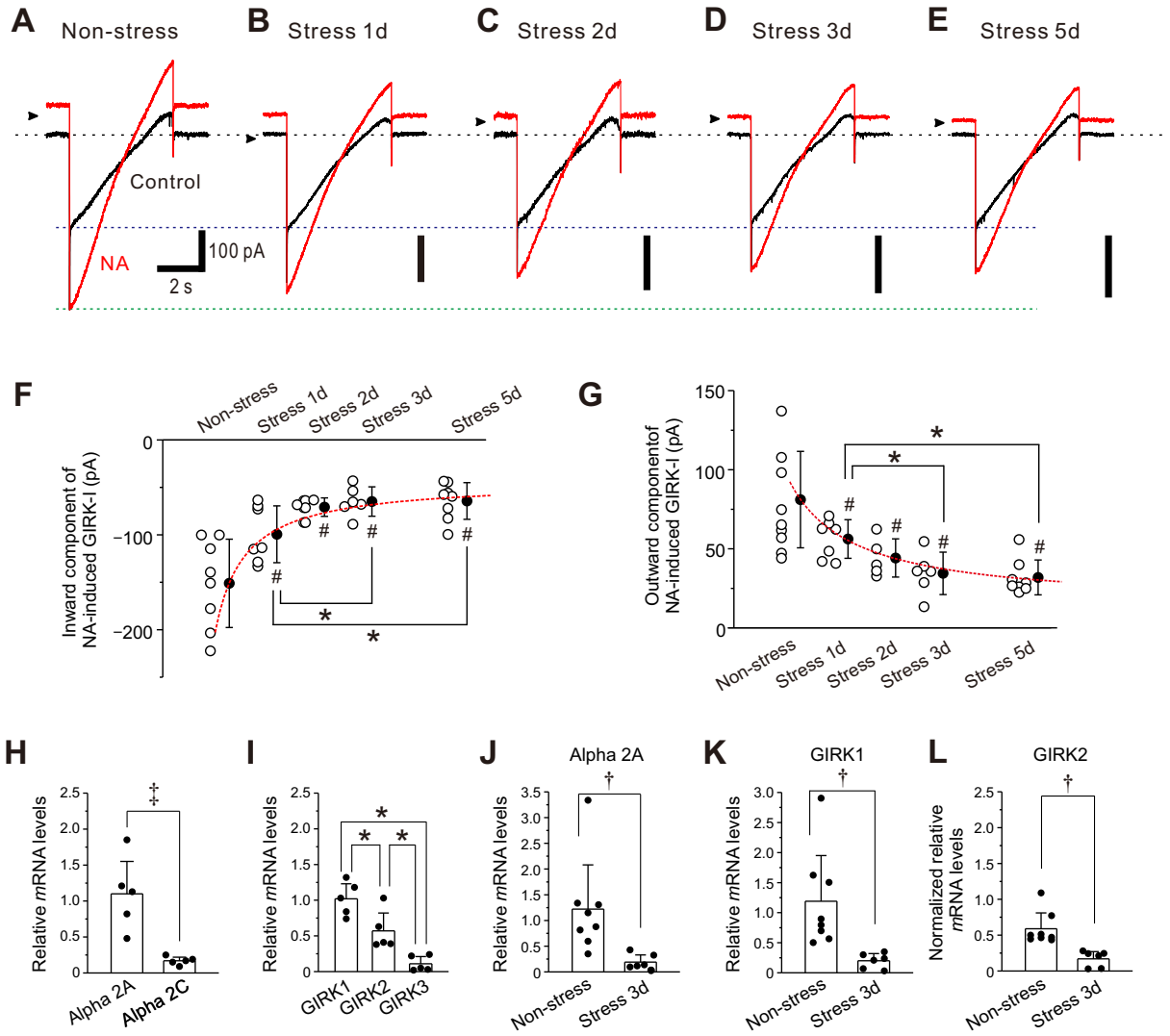
A
Non-stress
B
Stress 1d
C
Stress 2d
D
Stress 3d
E
Stress 5d
Control
NA
100 pA
2 s
F
Non-stress
Stress 1d
Stress 2d
Stress 3d
Stress 5d
Inward component of NA-induced GIRK-I (pA)
0
−100
−200
G
Outward componentof NA-induced GIRK-I (pA)
150
100
50
0
H
Relative mRNA levels
Alpha 2A
Alpha 2C
I
GIRK1
GIRK2
GIRK3
J
Alpha 2A
Non-stress
Stress 3d
K
GIRK1
L
GIRK2
Normalized relative mRNA levels

Figure 5

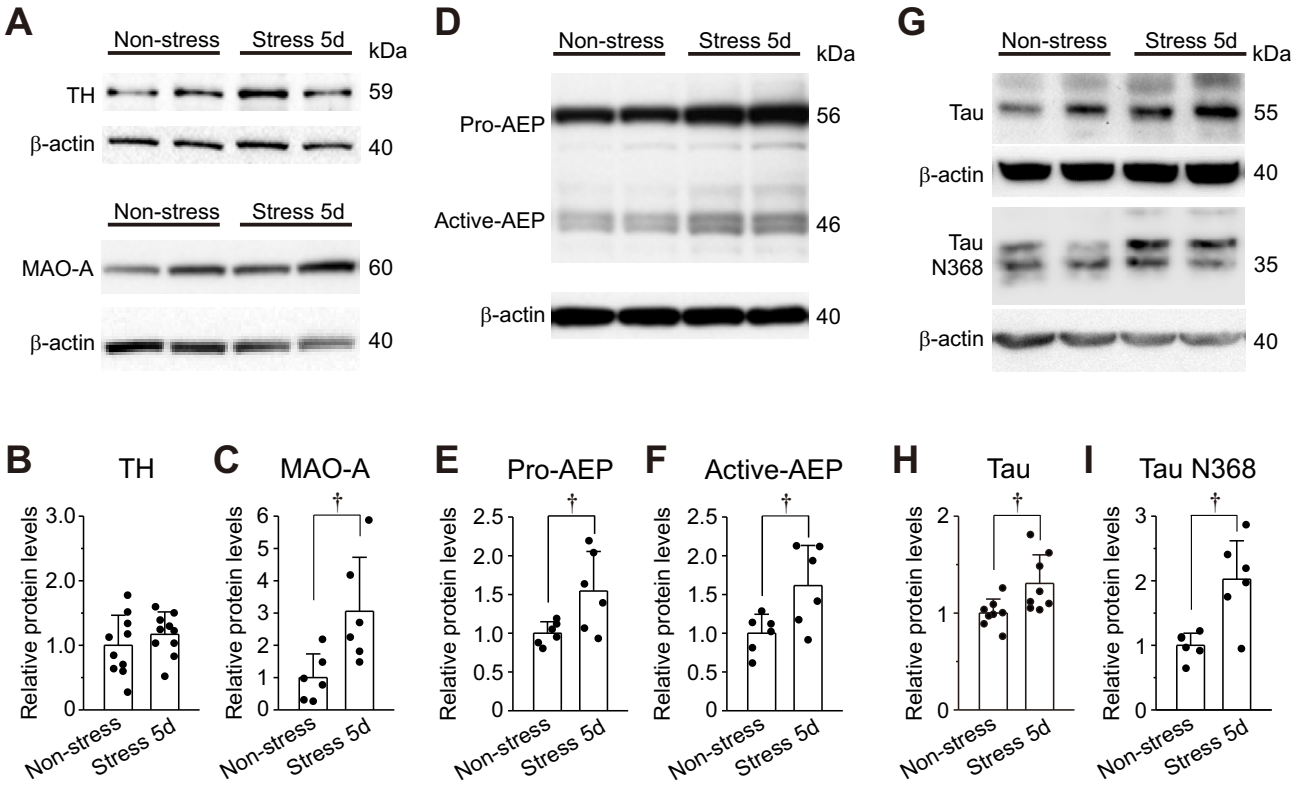
A
Non-stress
Stress 5d
kDa
TH
59
β-actin
40
Non-stress
Stress 5d
MAO-A
60
β-actin
40
D
Non-stress
Stress 5d
kDa
Pro-AEP
56
Active-AEP
46
β-actin
40
G
Non-stress
Stress 5d
kDa
Tau
55
β-actin
40
Tau
N368
35
β-actin
40
B
TH
C
MAO-A
E
Pro-AEP
F
Active-AEP
H
Tau
I
Tau N368
Relative protein levels
Non-stress
Stress 5d
†

Figure 6

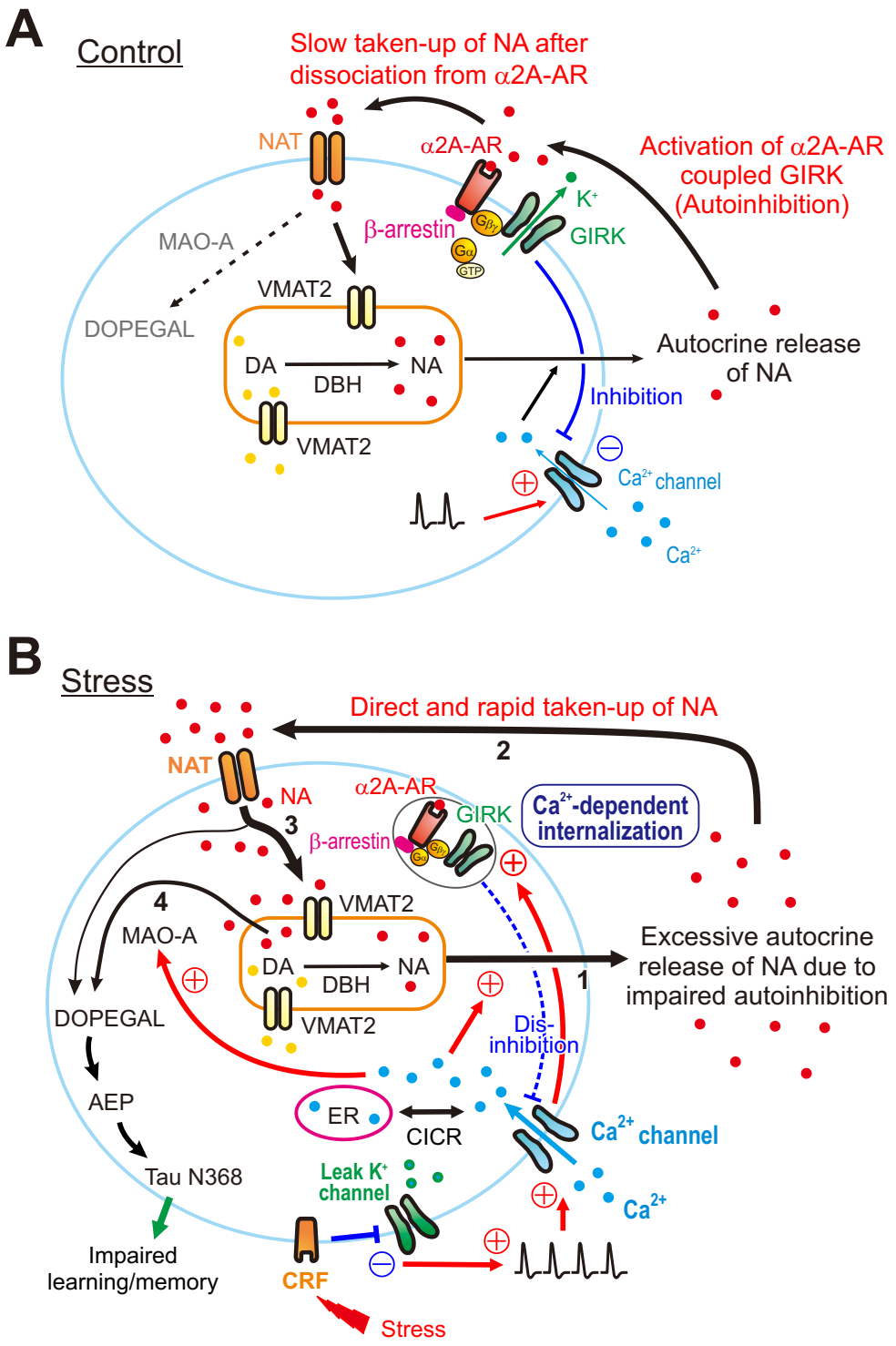
A
Control
Slow taken-up of NA after dissociation from α2A-AR
NAT
α2A-AR
Activation of α2A-AR coupled GIRK (Autoinhibition)
K+
GIRK
β-arrestin
Gβγ
Gα
GTP
MAO-A
VMAT2
DOPEGAL
DA
NA
DBH
Autocrine release of NA
Inhibition
VMAT2
Ca2+ channel
Ca2+
B
Stress
Direct and rapid taken-up of NA
2
NAT
NA
α2A-AR
GIRK
Ca2+-dependent internalization
3
β-arrestin
4
VMAT2
MAO-A
DA
NA
DBH
1
Excessive autocrine release of NA due to impaired autoinhibition
DOPEGAL
VMAT2
Dis-inhibition
AEP
ER
CICR
Ca2+ channel
Tau N368
Leak K+ channel
Ca2+
Impaired learning/memory
CRF
Stress